Interaction of Photons and Charged Particles with Matter

15

An x-ray image records variations in the passage of x rays through the body because of scattering and absorption. A side effect of making the image is the absorption of some x-ray or charged particle energy by the body. Radiation therapy depends on the absorption of large amounts of x-ray energy by a tumor. Diagnostic procedures in nuclear medicine (Chap. 17) introduce a small amount of radioactive substance in the body. Radiation from the radioactive nuclei is then detected. Some of the energy from the photons or charged particles emitted by the radioactive nucleus is absorbed in the body. To describe all of these effects requires that we understand the interaction of photons and charged particles with matter.

In Chap. 14 we discussed the transport of photons of ultraviolet and lower energy—a few electron volts or less. Now we will discuss the transport of photons of much higher energy—10 keV and above. We will also discuss the movement through matter of charged particles such as electrons, protons, and heavier ions. These high energy photons and charged particles are called *ionizing radiation*, because they produce ionization in the material through which they pass. The distinction is blurred, since ultraviolet light can also ionize.

A charged particle moving through matter loses energy by local ionization, disruption of chemical bonds, and increasing the energy of atoms it passes near. It is said to be *directly ionizing*. Photons passing through matter transfer energy to charged particles, which in turn affects the material. These photons are *indirectly ionizing*.

Photons and charged particles interact primarily with the electrons in atoms. Section 15.1 describes the energy levels of atomic electrons. Section 15.2 describes the various processes by which photons interact; these are elaborated in the next four sections, leading in Sect. 15.7 to the concept of a photon attenuation coefficient. Attenuation is extended to compounds and mixtures in Sect. 15.8.

An atom is often left in an excited state by a photon interaction. The mechanisms by which it loses energy are covered in Sect. 15.9. The energy that is transferred to electrons can cause radiation damage. The transfer process is described in Sects. 15.10 and 15.15–15.17.

Section 15.11 introduces the charged-particle stopping power, which is the rate of energy loss by a charged particle as it passes through a material. Extensions of this concept, which are important in radiation damage, are the linear energy transfer and the restricted collision stopping power, introduced in Sect. 15.12. A charged particle travels a certain distance through the material as it loses its kinetic energy. This leads in Sect. 15.13 to the concept of range. Charged particles also lose energy by emitting photons. The radiation yield is also discussed in Sect. 15.13. Insight into the process of radiation damage is gained by examining track structure in Sect. 15.14.

The last three sections return to the movement of energy from a photon beam to matter. The discussion requires an understanding of both photon interactions and charged-particle stopping power and range.

15.1 Atomic Energy Levels and X-ray Absorption

A neutral atom has a nuclear charge $+Ze$ surrounded by a cloud of Z electrons. As was described in Chap. 14, each electron has a definite energy, characterized by a set of five quantum numbers: n, l, s (which is always $\frac{1}{2}$), j, and m_j. (Instead of j and m_j, the numbers m_l and m_s are sometimes used.) There are restrictions on the values of the numbers:

$n = 1, 2, 3, \ldots$	the principal quantum number
$l = 0, 1, 2, \ldots, n-1$	the orbital angular momentum quantum number
$s = \frac{1}{2}$	the spin quantum number

R. K. Hobbie, B. J. Roth, *Intermediate Physics for Medicine and Biology*,
DOI 10.1007/978-3-319-12682-1_15,

$j = l - \frac{1}{2}$ or $l + \frac{1}{2}$, except that	the total angular
$j = \frac{1}{2}$ when $l = 0$	momentum quantum number
$m_j = -j, -(j-1), \ldots,$	"z component" of the total
$(j-1), j$	angular momentum

The dependence of the electron energy on m_j is very slight, unless the atom is in a magnetic field.

In each atom, only one electron can have a particular set of values of the quantum numbers. Since the atoms we are considering are not in a magnetic field, electrons with different values of m_j but the same values for n, l, and j will all be assumed to have the same energy. Electrons with different values of n are said to be in different *shells*. The shell for $n = 1$ is called the K shell; those for $n = 2, 3, 4, \ldots$ are labeled $L, M, N, \ldots$. Different values of l and j for a fixed value of n are called *subshells*, denoted by roman numeral subscripts on the shell labels. The maximum number of electrons that can be placed in a subshell is $2(2l + 1)$. Each electron bound to the atom has a certain negative energy, with zero energy defined when the electron is just unbound, that is, at rest infinitely far away from the atom. Table 15.1 lists the energy levels of electrons in tungsten. Some of the levels in Table 15.1 are shown in Fig. 15.1. The scale is logarithmic. Since the energies are negative, the magnitude increases in the downward direction. Tables of atomic energy levels can be found many places, including www.csrri.iit.edu/periodic-table.html .

The *ionization energy* is the energy required to remove the least-tightly-bound electron from the atom. For tungsten, it is about 6 eV. If one plots the ionization energy or the chemical valence of atoms as a function of Z, one finds abrupt changes when the last electron's value of n or l changes.

In contrast to this behavior of the outer electrons, the energy of an inner electron with fixed values of n and l varies smoothly with Z. To a first approximation, the two innermost K electrons are attracted to the nuclear charge Ze. The energy of the level can be estimated using Eq. 14.9 for hydrogen, with the nuclear charge e replaced by Ze:

$$E_K = -\frac{13.6Z^2}{1^2}. \qquad (15.1)$$

The two electrons also repel each other and experience some repulsion by electrons in other shells. This effect is called *charge screening*. Experiment (measuring values of E_K) shows that the effective charge seen by a K electron is approximately $Z_{\text{eff}} \approx Z - 2$ for heavy elements, so that for K electrons ($n = 1$),

$$E_K \approx -13.6(Z-2)^2 \qquad \text{(in eV)}. \qquad (15.2)$$

Table 15.1 Energy levels for electrons in a tungsten atom ($Z = 74$)

n	l	j	Number of electrons	X-ray label	Energy (eV)
1	0	$\frac{1}{2}$	2	K	−69 525
2	0	$\frac{1}{2}$	2	L_{I}	−12 100
	1	$\frac{1}{2}$	2	L_{II}	−11 544
	1	$\frac{3}{2}$	4	L_{III}	−10 207
3	0	$\frac{1}{2}$	2	M_{I}	−2 820
	1	$\frac{1}{2}$	2	M_{II}	−2 575
	1	$\frac{3}{2}$	4	M_{III}	−2 281
	2	$\frac{3}{2}$	4	M_{IV}	−1 872
	2	$\frac{5}{2}$	6	M_{V}	−1 809
4	0	$\frac{1}{2}$	2	N_{I}	−594
	1	$\frac{1}{2}$	2	N_{II}	−490
	1	$\frac{3}{2}$	4	N_{III}	−424
	2	$\frac{3}{2}$	4	N_{IV}	−256
	2	$\frac{5}{2}$	6	N_{V}	−244
	3	$\frac{5}{2}, \frac{7}{2}$	14	$N_{\text{VI,VII}}$	−35
5	0	$\frac{1}{2}$	2	O_{I}	−77
	1	$\frac{1}{2}$	2	O_{II}	−47
	1	$\frac{3}{2}$	4	O_{III}	−36
	2	$\frac{3}{2}, \frac{5}{2}$	4	$O_{\text{IV,V}}$	−6
6	0	$\frac{1}{2}$	2	P_{I}	

The screening is greater for electrons with larger values of n, which may be thought of as being in "orbits" of larger radius.

15.2 Photon Interactions

There are a number of different ways in which a photon can interact with an atom. The more important ones will be considered here. It is convenient to adopt a notation (γ, bc) where γ represents the incident photon and b and c are the results of the interaction. For example (γ, γ) represents initial and final photons having the same energy; in a (γ, e) interaction the photon is absorbed and only an electron emerges. This section describes the common interactions and the energy balance for each case.

15.2.1 Photoelectric Effect

In the *photoelectric effect,* (γ, e), the photon is absorbed by the atom and a single electron, called a *photoelectron*, is

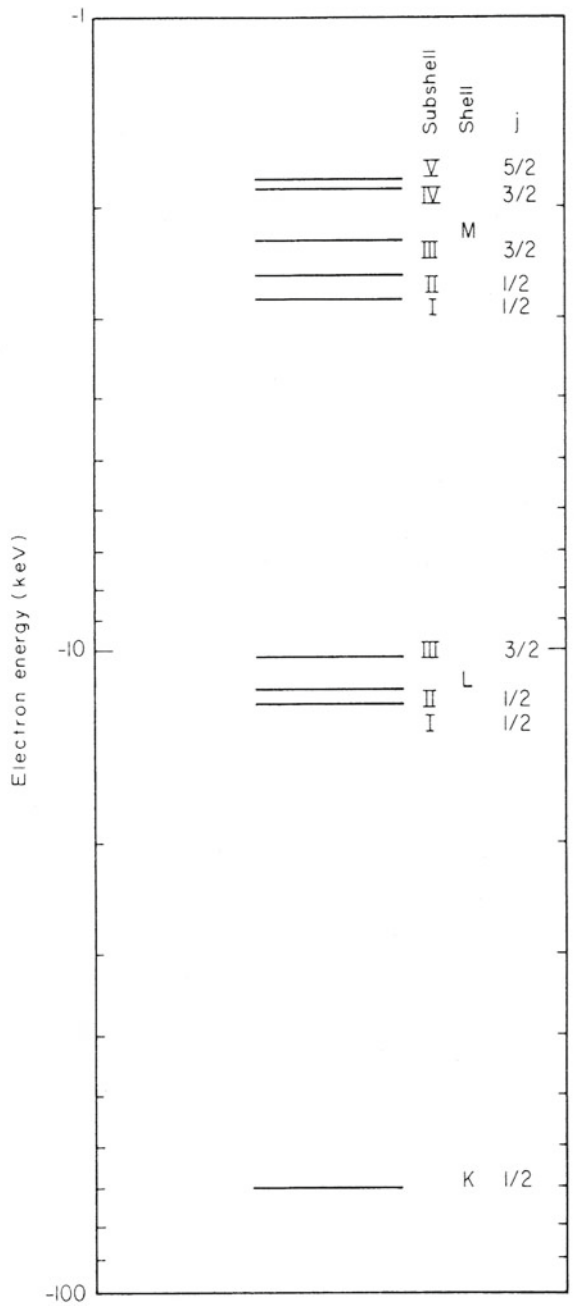

Fig. 15.1 Energy levels for electrons in tungsten

ejected. The initial photon energy $h\nu_0$ is equal to the final energy. The recoil kinetic energy of the atom is very small because its mass is large, so the final energy is the kinetic energy of the electron, T_{el}, plus the excitation energy of the atom. The excitation energy is equal to the binding energy of the ejected electron, B. The energy balance is therefore

$$h\nu_0 = T_{\text{el}} + B. \tag{15.3}$$

The atom subsequently loses its excitation energy. The deexcitation process described in Sect. 15.9 involves the emission of additional photons or electrons. The photoelectric cross section is τ.

15.2.2 Compton and Incoherent Scattering

In *Compton scattering*, $(\gamma, \gamma' e)$, the original photon disappears and a photon of lower energy and an electron emerge. The statement of energy conservation is

$$h\nu_0 = h\nu + T_{\text{el}} + B.$$

Usually the photon energy is high enough so that B can be neglected, and this is written as

$$h\nu_0 = h\nu + T_{\text{el}}. \tag{15.4}$$

The Compton cross section for scattering from a single electron is σ_C. *Incoherent scattering* is Compton scattering from all the electrons in the atom, with cross section σ_{incoh}.

15.2.3 Coherent Scattering

Coherent scattering is a (γ, γ) process in which the photon is elastically scattered from the entire atom. That is, the internal energy of the atom does not change. The recoil kinetic energy of the atom is very small (see Problem 8), and it is a good approximation to say that the energy of the incident photon equals the energy of the scattered photon:

$$h\nu_0 = h\nu. \tag{15.5}$$

The cross section for coherent scattering is σ_{coh}.

15.2.4 Inelastic Scattering

It is also possible for the final photon to have a different energy from the initial photon (γ, γ') without the emission of an electron. The internal energy of the target atom or molecule increases or decreases by a corresponding amount. Again, the recoil kinetic energy of the atom is negligible. Examples are fluorescence and Raman scattering. In fluorescence, if one waits long enough, additional photons are emitted, in which case the reaction could be denoted as $(\gamma, \gamma'\gamma'')$, or $(\gamma, 2\gamma)$, or even $(\gamma, 3\gamma)$.

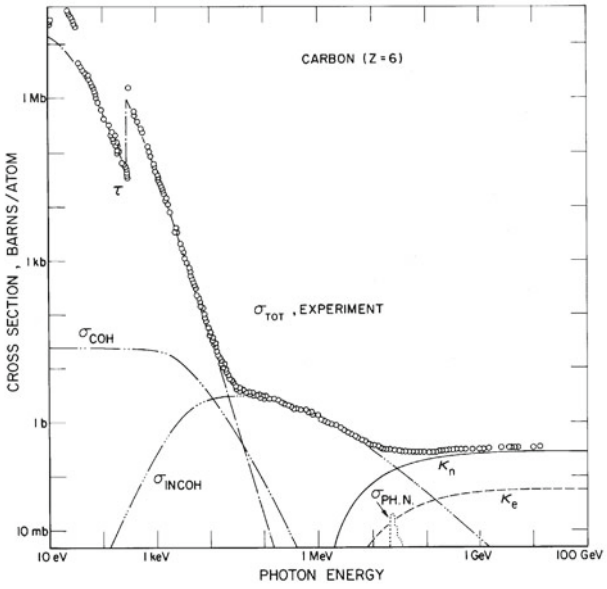

Fig. 15.2 Total cross section for the interactions of photons with carbon vs photon energy. The photoelectric cross section is τ, the coherent scattering cross section σ_{coh}, the total Compton cross section σ_{incoh}, and the nuclear and electronic (triplet) pair production are κ_n and κ_e. The photonuclear scattering cross section PHN is also shown. The cross section is given in barns: $1\,\text{b} = 10^{-28}\,\text{m}^2$. Reprinted with permission from Hubbell et al. (1980). Copyright 1980, American Institute of Physics. Figure courtesy of J. H. Hubbell

15.2.5 Pair Production

Pair production takes place at high energies. This is a (γ, e^+e^-) reaction. Since it takes energy to create the (negative) electron and the positive electron or *positron*, their rest energies must be included in the energy balance equation:

$$h\nu_0 = T_+ + m_e c^2 + T_- + m_e c^2 = T_+ + T_- + 2m_e c^2. \quad (15.6)$$

The cross section for pair production is κ.

15.2.6 Energy Dependence

Figure 15.2 shows the cross section for interactions of photons with carbon for photon energies from 10 to 10^{11} eV. At the lowest energies the photoelectric effect dominates. Between 10 keV and 10 MeV Compton scattering is most important. Above 10 MeV pair production takes over. There is a small bump at about 20 MeV due to nuclear effects, but its contribution to the cross section is only a few percent of that due to pair production. The four important effects are discussed in the next four sections.

15.3 The Photoelectric Effect

In the photoelectric effect a photon of energy $h\nu_0$ is absorbed by an atom, and an electron of kinetic energy $T_{\text{el}} = h\nu_0 - B$ is ejected. B is the magnitude of the binding energy of the electron and depends on which shell the electron was in. Therefore it is labeled B_K, B_L, and so forth. The cross section for the photoelectric effect, τ, is a sum of terms for each shell:

$$\tau = \tau_K + \tau_L + \tau_M + \cdots . \quad (15.7)$$

As the energy of a photon beam is decreased, the photoelectric cross section increases rapidly. For photon energies too small to remove an electron from the K shell, the cross section for the K-shell photoelectric effect is zero. Even though photons do not have enough energy to remove an electron from the K shell, they may have enough energy to remove L-shell electrons. The cross section for L electron photoelectric effect is much smaller than that for K electrons, but it increases with decreasing energy until its threshold energy is reached. This energy dependence is shown for lead in Fig. 15.3, which plots the cross section for the photoelectric effect, incoherent Compton scattering, and coherent scattering. The K absorption edge for the photoelectric effect is seen. The photoelectric effect below the K absorption edge is due to $L, M, \ldots$ electrons; above this energy the K electrons also participate. Above 0.8 MeV in lead Compton scattering becomes more important than the photoelectric effect.

The energy dependence of the photoelectric effect cross section is between E^{-2} and E^{-3}. An approximation to the Z and E dependence of the photoelectric cross section near 100 keV is (Attix 1986, p. 140)

$$\tau \propto Z^4 E^{-3}. \quad (15.8)$$

Once an atom has absorbed a photon and ejected a photoelectron, it is in an excited state. The atom will eventually lose this excitation energy by capturing an electron and returning to its ground state. The deexcitation processes are described in Sect. 15.9.

15.4 Compton Scattering

15.4.1 Kinematics

Compton scattering is a $(\gamma, \gamma' e)$ process. The equations that are used to relate the energy and angle of the emerging photon and electron, as well as the equations that give the cross section for the scattering, are usually derived assuming that the electron is free and at rest. We turn first to the kinematics.

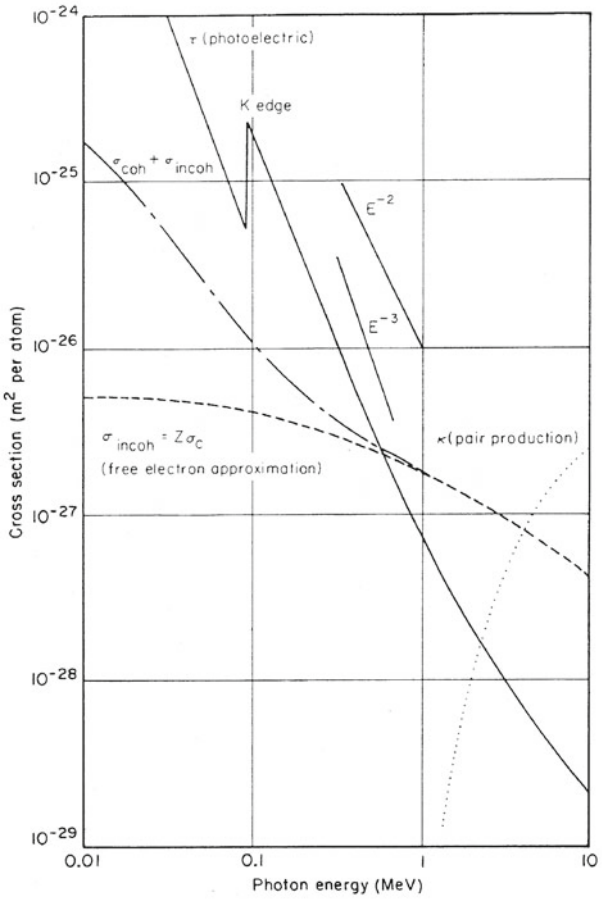

Fig. 15.3 Cross sections for the photoelectric effect and incoherent and coherent scattering from lead. The binding energies of the K and L shells are 0.088 and 0.0152 MeV. Plotted from Table 3.22 of Hubbell (1969)

A photon has energy E and momentum p, related by

$$E = h\nu = pc. \tag{15.9}$$

This is a special case of a more general relationship from special relativity:

$$E^2 = (pc)^2 + (m_0c^2)^2. \tag{15.10}$$

In these equations E is the total energy of the particle, p its momentum, m_0 the *rest mass* of the particle (measured when it is not moving), and m_0c^2 is the *rest energy*.[1] For a photon, which can never be at rest, $m_0 = 0$. Equation 15.9 can also be derived from the classical electromagnetic theory of light.

The conservation of energy and momentum can be used to derive the relationship between the angle at which the scattered photon emerges and its energy. A detailed knowledge of the forces involved is necessary to calculate the relative number of photons scattered at different angles; in fact, this calculation must be done using quantum mechanics. Figure 15.4 shows the geometry of the scattering. The electron emerges with momentum p, kinetic energy T, and total energy $E = T + m_ec^2$. It emerges at an angle ϕ with the direction of the incident photon. The scattered photon emerges at angle θ with a reduced energy and a corresponding frequency ν' which is lower than ν_0, the frequency of the incident photon. Conservation of momentum in the direction of the incident photon gives

Fig. 15.4 Momentum relationships in Compton scattering. **a** Before. **b** After. The photon emerges at angle θ, the electron at angle ϕ

$$\frac{h\nu_0}{c} = \frac{h\nu'}{c}\cos\theta + p\cos\phi,$$

while conservation of momentum at right angles to that direction gives

$$\frac{h\nu'}{c}\sin\theta = p\sin\phi.$$

Conservation of energy gives

$$h\nu_0 = h\nu' + T.$$

The equation $E = T + m_ec^2$ can be combined with Eq. 15.10 to give

$$(pc)^2 = T^2 + 2m_ec^2T.$$

The last four equations can then be combined and solved for various unknowns.

The wavelength of the scattered photon is

$$\lambda' - \lambda_0 = \frac{c}{\nu'} - \frac{c}{\nu_0} = \frac{h}{m_ec}(1 - \cos\theta). \tag{15.11}$$

The wavelength shift (but not the frequency or energy shift) is independent of the incident wavelength. The quantity h/m_ec has the dimensions of length and is called the *Compton wavelength* of the electron. Its numerical value is

$$\lambda_C = \frac{h}{m_ec} = 2.427 \times 10^{-12}\ \text{m} = 2.427\ \text{pm}. \tag{15.12}$$

[1] Since this is one of the few relativistic results we will need, it is not developed here. A discussion can be found in any book on special relativity.

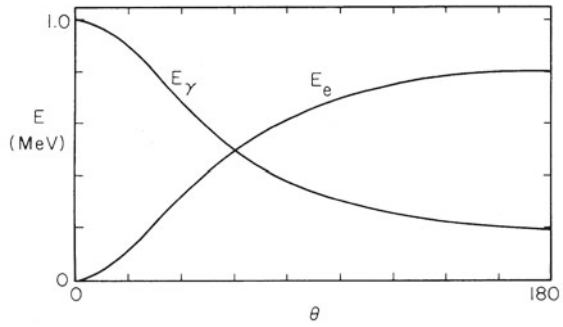

Fig. 15.5 The energy of the emerging photon and recoil electron as a function of θ, the angle of the emerging photon, for a 1-MeV incident photon

If Eq. 15.11 is solved for the energy of the scattered photon, the result is

$$h\nu' = \frac{h\nu_0}{1 + x(1 - \cos\theta)}, \tag{15.13}$$

where x is the energy of the incident photon in units of $m_e c^2 = 511$ keV:

$$x = \frac{h\nu_0}{m_e c^2}. \tag{15.14}$$

The energy of the recoil electron is $T = h\nu_0 - h\nu'$:

$$T = \frac{h\nu_0 x(1 - \cos\theta)}{1 + x(1 - \cos\theta)}. \tag{15.15}$$

Figure 15.5 shows the energy of the scattered photon and the recoil electron as a function of θ, the angle of emergence of the photon. The sum of the two energies is 1 MeV, the energy of the incident photon.

15.4.2 Cross Section: Klein–Nishina Formula

The inclusion of dynamics, which allows us to determine the relative number of photons scattered at each angle, is fairly complicated. The quantum-mechanical result is known as the *Klein–Nishina* formula (Attix 1986). The result depends on the polarization of the photons. For unpolarized photons, the cross section per unit solid angle for a photon to be scattered at angle θ is

$$\frac{d\sigma_C}{d\Omega} = \frac{r_e^2}{2}\left[\frac{1 + \cos^2\theta + \dfrac{x^2(1 - \cos\theta)^2}{1 + x(1 - \cos\theta)}}{[1 + x(1 - \cos\theta)]^2}\right], \tag{15.16}$$

where

$$r_e = \frac{e^2}{4\pi\epsilon_0 m_e c^2} = 2.818 \times 10^{-15}\,\text{m},$$

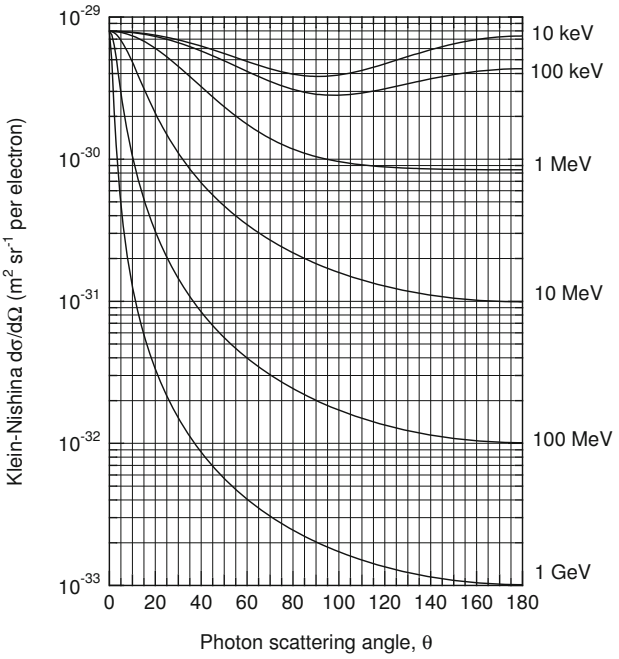

Fig. 15.6 Differential cross section for Compton scattering of unpolarized photons from a free electron, calculated from Eq. 15.16. The incident photon energy for each curve is shown on the right

is the *classical radius* of the electron. The cross section is plotted in Fig. 15.6. It is peaked in the forward direction at high energies. As $x \to 0$ (long wavelengths or low energy) it approaches

$$\frac{d\sigma_C}{d\Omega} = \frac{r_e^2(1 + \cos^2\theta)}{2}, \tag{15.17}$$

which is symmetric about 90°.

Equation 15.16 can be integrated over all angles to obtain the total Compton cross section for a single electron:

$$\sigma_C = 2\pi r_e^2\left[\frac{1 + x}{x^2}\left(\frac{2(1 + x)}{1 + 2x} - \frac{\ln(1 + 2x)}{x}\right) + \frac{\ln(1 + 2x)}{2x} - \frac{1 + 3x}{(1 + 2x)^2}\right]. \tag{15.18}$$

As $x \to 0$, this approaches

$$\sigma_C \to \frac{8\pi r_e^2}{3} = 6.652 \times 10^{-29}\,\text{m}^2. \tag{15.19}$$

Figure 15.7 shows σ_C as a function of energy.

The classical analog of Compton scattering is *Thomson scattering* of an electromagnetic wave by a free electron. The electron experiences the electric field $\mathbf{E}$ of an incident plane electromagnetic wave and therefore has an acceleration $-e\mathbf{E}/m$. Accelerated charges radiate electromagnetic waves, and the energy radiated in different directions can be

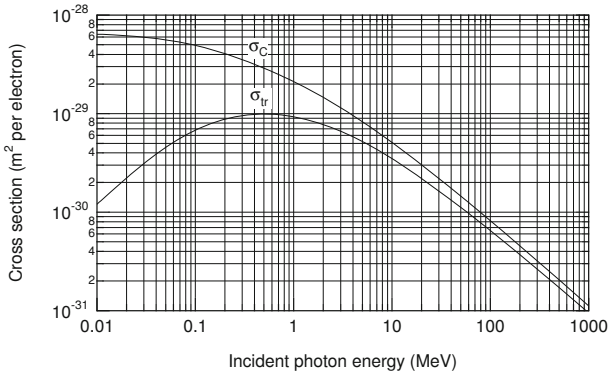

Fig. 15.7 The total cross section σ_C for Compton scattering by a single electron and the cross section for energy transfer $\sigma_{\rm tr} = f_C\sigma_C$

calculated, giving Eqs. 15.17 and 15.19. (See, for example, Jackson 1999, Chap. 14.) In the classical limit of low photon energies and momenta, the energy of the recoil electron is negligible.

15.4.3 Incoherent Scattering

The Compton cross section is for a single electron. For an atom containing Z electrons, the maximum value of the incoherent cross section occurs if all Z electrons take part in the Compton scattering:

$$\sigma_{\rm incoh} \le Z\sigma_C.$$

For carbon $Z\sigma_C = 4.0\times10^{-28}$ m^2. This value is approached by $\sigma_{\rm incoh}$ near 10 keV. At low energies $\sigma_{\rm incoh}$ falls below this maximum value because the electrons are bound and not at rest. This falloff can be seen in Fig. 15.2. It is appreciable for energies as high as 7–8 keV, even though the K-shell binding energy in carbon is only 283 eV. The electron motion and binding in the target atom also cause a small spread in the energy of the scattered photons (Carlsson et al. 1982).

Departures of the angular distribution and incoherent cross section from Z times the Klein–Nishina formula are discussed by Hubbell et al. (1975) and by Jackson and Hawkes (1981).

15.4.4 Energy Transferred to the Electron

We will need to know the average energy transferred to an electron in a Compton scattering. Equation 15.15 gives the electron kinetic energy as a function of photon scattering angle. The transfer cross section is defined to be

$$\sigma_{\rm tr} = \int_0^\pi \frac{d\sigma_C}{d\Omega}\frac{T(\theta)}{h\nu_0}2\pi\sin\theta\,d\theta = f_C\sigma_C. \qquad (15.20)$$

This can be integrated. The result is (see Attix 1986, p. 134)

$$\sigma_{\rm tr} = 2\pi r_e^2\left[\frac{2(1+x)^2}{x^2(1+2x)} - \frac{1+3x}{(1+2x)^2} - \frac{(1+x)(2x^2-2x-1)}{x^2(1+2x)^2} - \frac{4x^2}{3(1+2x)^3} - \left(\frac{1+x}{x^3} - \frac{1}{2x} + \frac{1}{2x^3}\right)\ln(1+2x)\right]. \qquad (15.21)$$

This quantity is also plotted in Fig. 15.7. Equation 15.21 is a rather nasty equation to evaluate, particularly at low energies, because many of the terms nearly cancel.

15.5 Coherent Scattering

A photon can also scatter elastically from an atom, with none of the electrons leaving their energy levels. This (γ,γ) process is called *coherent scattering* (sometimes called *Rayleigh scattering*), and its cross section is $\sigma_{\rm coh}$. The entire atom recoils; if one substitutes the atomic mass in Eqs. 15.14 and 15.15, one finds that the atomic recoil kinetic energy is negligible.

The primary mechanism for coherent scattering is the oscillation of the electron cloud in the atom in response to the electric field of the incident photons. There are small contributions to the scattering from nuclear processes. The cross section can be calculated classically as an extension of Thomson scattering, or it can be done using various degrees of quantum-mechanical sophistication (Kissel et al. 1980).

The coherent cross section is peaked in the forward direction because of interference effects between electromagnetic waves scattered by various parts of the electron cloud. The peak is narrower for elements of lower atomic number and for higher energies. Coherent and incoherent scattering cross sections are shown in Fig. 15.8 for 100-keV photons scattering from carbon, calcium and lead. Also shown for comparison is $Z(d\sigma/d\Omega)_{KN}$.

If the wavelength of the incident photon is large compared to the size of the atom, then all Z electrons behave like a single particle with charge $-Ze$ and mass Zm_e. The classical radius is replaced by $Z^2e^2/4\pi\epsilon_0 Zm_ec^2$. From Eqs. 15.17 and 15.19, one can see that the cross section in this limit is Z^2 times the single-electron value: $Z^2\sigma_C$. The limiting value for carbon is 2.39×10^{-27} m^2, which can be compared to the low energy limit for $\sigma_{\rm coh}$ in Fig. 15.2.

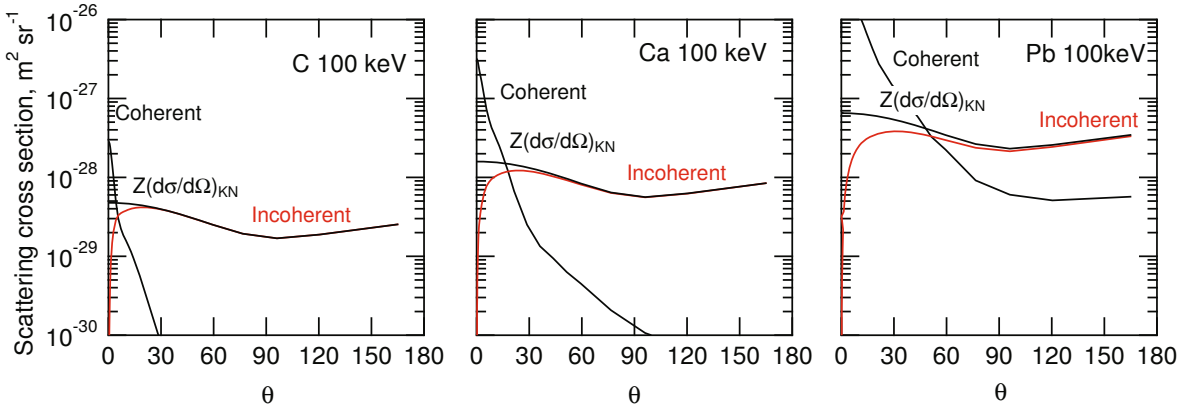

Fig. 15.8 The coherent and incoherent differential cross sections as a function of angle for 100-keV photons scattering from carbon, calcium, and lead. Calculated from Hubbell et al. (1975)

15.6 Pair Production

A photon with energy above 1.02 MeV can produce a particle–antiparticle pair: a negative electron and a positron. Conservation of energy requires that

$$h\nu_0 = \underbrace{T_- + m_e c^2}_{\text{electron}} + \underbrace{T_+ + m_e c^2}_{\text{positron}} = T_+ + T_- + 2m_e c^2. \tag{15.22}$$

Since the rest energy ($m_e c^2$) of an electron or positron is 0.51 MeV, pair production is energetically impossible for photons below $2m_e c^2 = 1.02$ MeV.

One can show, using $h\nu_0 = pc$ for the photon, that momentum is not conserved by the positron and electron if Eq. 15.22 is satisfied. Pair production always takes place in the Coulomb field of another particle (usually a nucleus) that recoils to conserve momentum. The nucleus has a large mass, so its kinetic energy $p^2/2m$ is small compared to the terms in Eq. 15.22. The cross section for this (γ, e^+e^-) reaction involving the nucleus is κ_n.

An additional contrbution to the cross section, κ_e, arises when the incident photon energy exceeds $4m_e c^2 = 2.04$ MeV, the threshold for pair production in which a free electron (rather than a nucleus) recoils to conserve momentum. Because ionization and free-electron pair production are $(\gamma, e^-e^-e^+)$ processes, this is usually called *triplet production*. Extensive data are given in Hubbell et al. (1980).

The cross section for both processes is $\kappa = \kappa_n + \kappa_e$. The energy dependence of κ can be seen in Figs. 15.1 and 15.2.

15.7 The Photon Attenuation Coefficient

Consider the arrangement shown in Fig. 15.9a, in which a beam of photons is collimated so that a narrow beam strikes a detector. A scattering material is then introduced in the beam.

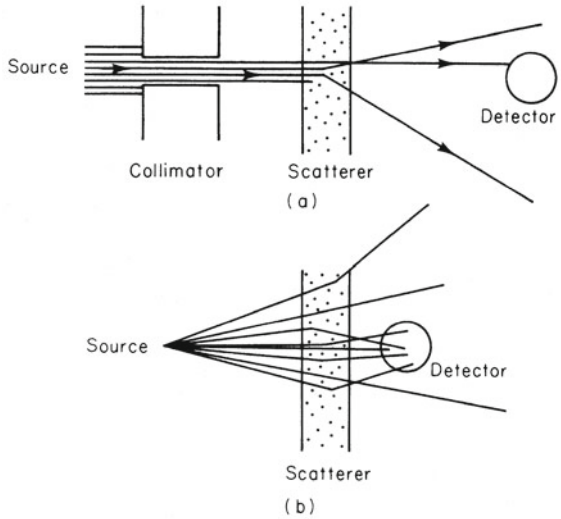

Fig. 15.9 Measurements with narrow-beam geometry (**a**) and broad-beam geometry (**b**)

Some of the photons pass through the material without interaction. Others are scattered. Still others disappear because of photoelectric effect or pair-production interactions. If we measure only photons that remain in the unscattered beam, the loss of photons is called *attenuation* of the beam. Attenuation includes both scattering and absorption. We record as still belonging to the beam only photons that did not interact; they still travel in the forward direction with the original energy. This is called a *narrow-beam geometry* measurement. It is an idealization, because photons that undergo Compton or coherent scattering through a small angle can still strike the detector. Figure 15.9b shows a source, scatterer, and detector geometry that is much more difficult to interpret. In this case photons that are initially traveling in a different direction are scattered into the detector. These are called *broad-beam geometry* experiments.

In narrow-beam geometry, the total cross section is related to the total number of particles that have interacted in the scatterer. Let N be the number of particles that have not undergone any interaction in passing through scattering material of thickness z. We saw in Sect. 14.5 that the number of particles that have not interacted decreases in thickness dz by

$$dN = -\frac{\sigma_{\text{tot}} N_A \rho}{A} N\, dz,$$

so that

$$\frac{dN}{dz} = -\mu_{\text{atten}} N,$$

where

$$\mu_{\text{atten}} = \frac{N_A \rho \sigma_{\text{tot}}}{A}. \tag{15.23}$$

In these equations ρ is the mass density of the target material and A is its atomic weight.[2] The number of particles that have undergone no interaction decays exponentially with distance:

$$N(z) = N_0 e^{-\mu_{\text{atten}} z}. \tag{15.24}$$

The quantity μ_{atten} is called the *total linear attenuation coefficient*.

In a broad-beam geometry configuration the total number of photons reaching the detector includes secondary photons and is larger than the value given by Eq. 15.24.

The units in Eqs. 15.23 and 15.24 are worth discussing. Avogadro's number is 6.022×10^{23} entities mol^{-1}. If the density ρ is in kg m^{-3} and σ_{tot} is in m^2, then A must be expressed in kg mol^{-1} and μ_{atten} is in m^{-1}. On the other hand, it is possible to express ρ in g cm^{-3}, σ_{tot} in cm^2, and A in g mol^{-1}, so that μ_{atten} is in cm^{-1}. As an example, consider carbon, for which $A = 12.011 \times 10^{-3}$ kg mol^{-1} $= 12.011$ g mol^{-1}. If $\sigma_{\text{tot}} = 1.269 \times 10^{-28}$ m^2 atom^{-1} $= 1.269 \times 10^{-24}$ cm^2 atom^{-1}, then either

$$\begin{aligned}\mu_{\text{atten}} &= \frac{(6.022 \times 10^{23}\,\text{atom mol}^{-1})(2.000 \times 10^{3}\,\text{kg m}^{-3})}{12.011 \times 10^{-3}\,\text{kg mol}^{-1}} \\ &\quad \times (1.269 \times 10^{-28}\,\text{m}^2\,\text{atom}^{-1}) \\ &= 12.7\,\text{m}^{-1}\end{aligned}$$

or

$$\begin{aligned}\mu_{\text{atten}} &= \left(\frac{(6.022 \times 10^{23}\,\text{atom mol}^{-1})(2.000\,\text{g cm}^{-3})}{12.011\,\text{g mol}^{-1}}\right) \\ &\quad \times (1.269 \times 10^{-24}\,\text{cm}^2\,\text{atom}^{-1}) \\ &= 0.127\,\text{cm}^{-1}.\end{aligned}$$

[2] The atomic weight is potentially confusing. Sometimes A has no units (as in labeling an nuclear isotope), sometimes it is in grams per mole, and sometimes it is in kilograms per mole).

The total cross section for photon interactions is

$$\sigma_{\text{tot}} = \sigma_{\text{coh}} + \sigma_{\text{incoh}} + \tau + \kappa. \tag{15.25a}$$

In many situations the coherently scattered photons cannot be distinguished from those unscattered, and σ_{coh} should not be included:

$$\sigma_{\text{tot}} = \sigma_{\text{incoh}} + \tau + \kappa. \tag{15.25b}$$

Tables usually include total cross sections and attenuation coefficients both with and without coherent scattering.

It is possible to regroup the terms in Eqs. 15.23 and 15.24 in a slightly different way:

$$dN = -N \frac{N_A \sigma_{\text{tot}}}{A} \rho dz.$$

The quantity $N_A \sigma_{\text{tot}}/A$ is the *mass attenuation coefficient*, μ_{atten}/ρ (m^2 kg^{-1}):

$$\frac{\mu_{\text{atten}}}{\rho} = \frac{N_A \sigma_{\text{tot}}}{A}. \tag{15.26}$$

The exponential attenuation is then

$$N(\rho z) = N_0 e^{-(\mu_{\text{atten}}/\rho)(\rho z)}. \tag{15.27}$$

The mass attenuation coefficient has the advantage of being independent of the density of the target material, which is particularly useful if the target is a gas. It has an additional advantage if Compton scattering is the dominant interaction. If $\sigma_{\text{tot}} = Z\sigma_C$, then

$$\frac{\mu_{\text{atten}}}{\rho} = \frac{Z \sigma_C N_A}{A}.$$

Since Z/A is nearly $1/2$ for all elements except hydrogen, this quantity changes very little throughout the periodic table. This constancy is not true for the photoelectric effect or pair production. Figure 15.10 plots the mass attenuation coefficient vs energy for three substances spanning the periodic table. It is nearly independent of Z around 1 MeV where Compton scattering is dominant. The K and L absorption edges can be seen for lead; for the lighter elements they are below 10 keV. Figure 15.11 shows the contributions to μ_{atten}/ρ for air from the photoelectric effect, incoherent scattering, and pair production. Tables of mass attenuation coefficients are provided by the National Institute of Standards and Technology (NIST) at http://www.nist.gov/pml/data/xcom/index.cfm.

15.8 Compounds and Mixtures

The usual procedure for dealing with mixtures and compounds is to assume that each atom scatters independently.

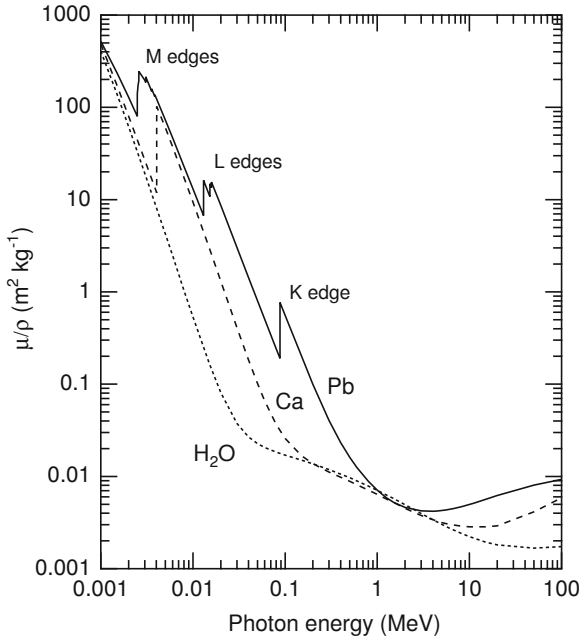

Fig. 15.10 Mass attenuation coefficient vs. energy for lead, calcium, and water. Near 1 MeV the mass attenuation coefficient is nearly independent of Z. (Plotted from data provided by NIST: http://www.nist.gov/pml/data/xcom/index.cfm)

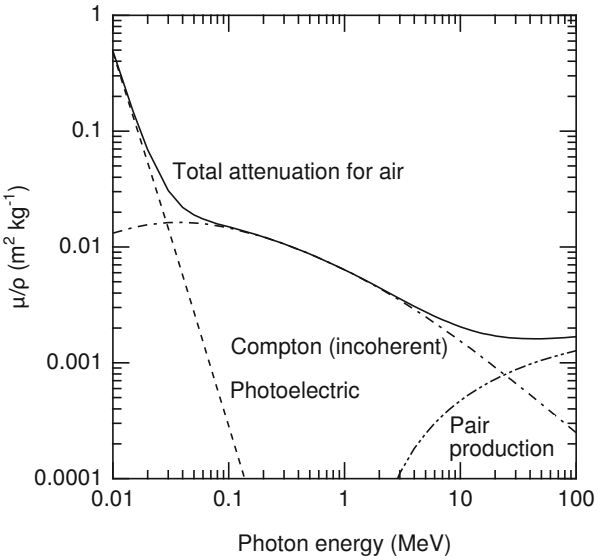

Fig. 15.11 Mass attenuation coefficient vs energy for air. (Plotted from data provided by NIST: http://www.nist.gov/pml/data/xcom/index.cfm)

If the cross section for element i summed over all the interaction processes of interest is denoted by σ_i, then Eq. 14.19 is replaced by

$$\frac{\overline{n}}{N} = \sum_i (N_T)_i \sigma_i = \left(\sum_i (N_{TV})_i \sigma_i \right) dz, \qquad (15.28)$$

where $(N_T)_i$ is the number of target atoms of species i *per unit projected area* of the target and $(N_{TV})_i$ is the number of target atoms *per unit volume*. The sum is taken over all elements in the compound or mixture.

It is possible to replace the sum by the product of the cross section per molecule multiplied by the number of molecules per unit volume. The cross section per molecule is the sum of the cross sections for all the atoms in the molecule. To see that this is so, note that a volume of scatterer V contains a total mass $M = \rho V$. The mass of each element is M_i and the mass fraction is $w_i = M_i/M$. The total number of atoms of species i in volume V is the number of moles times Avogadro's number:

$$(N_{TV})_i = \frac{M_i N_A}{A_i V} = \frac{w_i}{A_i} \rho N_A. \qquad (15.29)$$

The mass fraction of element i in a compound containing a_i atoms per molecule with atomic mass A_i is

$$w_i = \frac{a_i A_i}{A_{\text{mol}}}, \qquad (15.30)$$

where A_{mol} is the molecular weight. Therefore

$$\sum_i (N_{TV})\sigma_i = \left(\sum_i \frac{a_i \sigma_i}{A_{\text{mol}}} \right) \rho N_A$$
$$= \left(\sum_i a_i \sigma_i \right) \frac{\rho N_A}{A_{\text{mol}}} = \sigma_{\text{mol}} (N_{TV})_{\text{mol}}. \qquad (15.31)$$

The factor $(N_{TV})_{\text{mol}} = \rho N_A / A_{\text{mol}}$ is the number of molecules per unit volume. When a target entity (molecule) consists of a collection of subentities (atoms), we can say that in this approximation (all subentities interacting independently), the cross section per entity is the sum of the cross sections for each subentity. For example, for the molecule CH_4, the total molecular cross section is $\sigma_{\text{carbon}} + 4\sigma_{\text{hydrogen}}$ and the molecular weight is $[(4 \times 1) + 12 = 16] \times 10^{-3}$ kg mol^{-1}.

15.9 Deexcitation of Atoms

After the photoelectric effect, Compton scattering, or triplet production, an atom is left with a hole in some electron shell. An atom can be left in a similar state when an electron is knocked out by a passing charged particle or by certain transformations in the atomic nucleus that are discussed in Chap. 17.

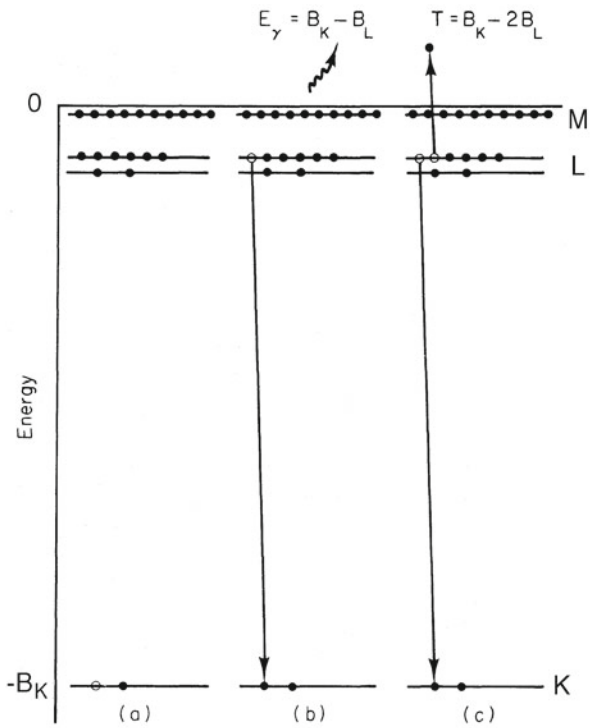

Fig. 15.12 Two possible mechanisms for the deexcitation of an atom with a hole in the K shell. **a** The atom with the hole in the K shell. **b** An electron has moved from the L shell to the K shell with emission of a photon of energy $B_K - B_L$. **c** An electron has moved from the L shell to the K shell. The energy liberated is taken by another electron from the L shell, which emerges with energy $B_K - 2B_L$. This electron is called an Auger electron

The hole in the shell can be filled by two competing processes: a *radiative transition*, in which a photon is emitted as an electron falls into the hole from a higher level, or a *nonradiative* or *radiationless transition*, such as the emission of an *Auger electron* from a higher level as a second electron falls from a higher level to fill the hole. Both processes are shown in Fig. 15.12. In the radiative transition, the energy of the photon is equal to the difference in binding energies of the two levels. For the example of Fig. 15.12b, the photon energy is $B_K - B_L$. The emission of an L-shell Auger electron is shown in Fig. 15.12c: its energy is $T = (B_K - B_L) - B_L = B_K - 2B_L$. Table 15.2 shows the energy changes that occur after a hole is created in an atom by photoelectric excitation. It is worth understanding each table entry in detail. Two different paths for deexcitation are shown: one for photon emission and one for ejection of an Auger electron. The sum of the photon, electron, and atomic excitation energies does not change.

The photon that is emitted is called a *characteristic photon* or a *fluorescence photon*. Its energy is given by the difference of two electron energy levels in the atom. There is an historical nomenclature for these photons. Because a hole moving to larger values of n corresponds to a decrease in the total energy of an atom, it is customary to draw the energy levels for holes instead of electrons, as in Fig. 15.13. Transitions in which the hole is initially in the $n = 1$ state give rise to the K series of x rays, those in which the initial hole is in the $n = 2$ state give rise to the L series, and so on. Greek letters (and their subscripts) are used to denote the shell (and subshell) of the final hole. The transitions shown in Fig. 15.13 are consistent with certain selection rules which can be derived using quantum theory:

$$\Delta l = \pm 1, \qquad \Delta j = 0, \pm 1. \tag{15.32}$$

We saw in Eqs. 15.1 and 15.2 that the position of a level could be estimated by the Bohr formula corrected for screening. The energy of the K_α line—which depends on screening for both the initial ($n = 2$) and final ($n = 1$) values of $n$can be fitted empirically by

$$E_{K_\alpha} = \left(\tfrac{3}{4}\right)(13.6)(Z-1)^2. \tag{15.33}$$

After creation of a hole in the K shell, it is random whether the atom deexcites by emitting a photon or an Auger electron. The probability of photon emission is called the *fluorescence yield*, W_K. The Auger yield is $A_K = 1 - W_K$. For a vacancy in the L or higher shells, one must consider the fluorescence yield for each subshell, defined as the number of photons emitted with an initial state corresponding to a hole in a subshell, divided by the number of holes in that subshell. The situation is further complicated by the fact that radiationless transitions can take place within the subshell, thereby altering the number of vacancies in each subshell. These are called *Coster–Kronig transitions,* and they are also accompanied by the emission of an electron. For example, a hole in the L_I shell can be filled by an electron from the L_III shell with the ejection of an M-shell electron. A *super–Coster–Kronig transition* involves electrons all within the same shell, for example, a hole in the M_I shell filled by an electron from the M_II shell with the ejection of an electron from the M_IV shell.

One can define an average fluorescence yield $\overline{W}_L$, $\overline{W}_M$, etc. for each shell, but it is not a fundamental property of the atom, since it depends on the vacancy distribution in the subshells. Bambynek et al. (1972) review the physics of atomic deexcitations and present theoretical and experimental data for the fundamental parameters. They show that $\overline{W}_L$ is less sensitive to the initial vacancy distribution than one might expect, because of the rapid changes in hole distribution caused by the Coster–Kronig transitions. Hubbell et al. (1994) provide a more recent review. Figure 15.14 shows values for W_K, $\overline{W}_L$, and $\overline{W}_M$ as a function of Z. One can see from this figure that radiationless transitions are much more important

Table 15.2 Energy changes in the photoelectric effect and in subsequent deexcitation

Process	Total photon energy	Total electron energy	Atom excitation energy	Sum
Before photon strikes atom	$h\nu$	0	0	$h\nu$
After photoelectron is ejected (Fig. 15.12)	0	$h\nu - B_K$	B_K	$h\nu$
Case 1: Deexcitation by the emission of a K and an L photon				
Emission of K fluorescence photon (Fig. 15.12b)	$B_K - B_L$	$h\nu - B_K$	B_L	$h\nu$
Emission of L fluorescence photon	$B_K - B_L, B_L$	$h\nu - B_K$	0	$h\nu$
Case 2: Deexcitation by emission of an Auger electron from the L shell				
Emission of Auger electron (Fig. 15.12c)	0	$h\nu - B_K, B_K - 2B_L$	$2B_L$	$h\nu$
First L-shell hole filled by fluorescence	B_L	$h\nu - B_K, B_K - 2B_L$	B_L	$h\nu$
Second L-shell hole filled by fluorescence	B_L, B_L	$h\nu - B_K, B_K - 2B_L$	0	$h\nu$

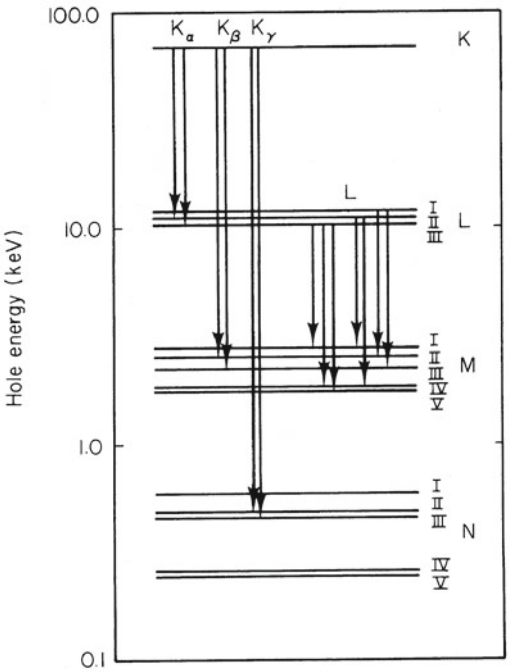

Fig. 15.13 Energy-level diagram for holes in tungsten, and some of the x-ray transitions

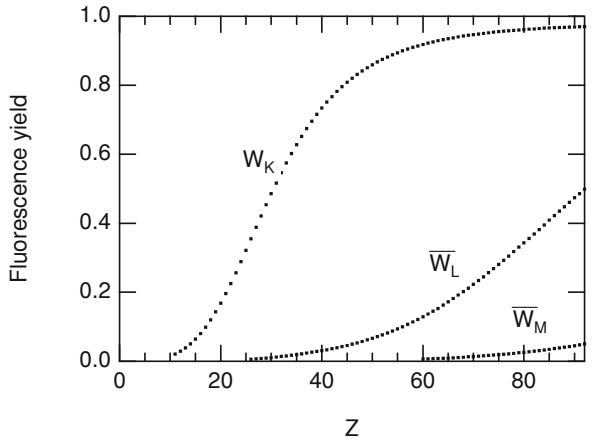

Fig. 15.14 Fluorescence yields for K-, L-, and M-shell vacancies as a function of atomic number Z. Points are from Table 8 of Hubbell et al. (1994)

(the fluorescent yield is much smaller) for the L shell than for the K shell. They are nearly the sole process for higher shells. The deexcitation is often called the *Auger cascade*.

The Auger cascade produces many vacancies in the outer shells of the atom, and some of these may be filled by electrons from other atoms in the same molecule. This process can break molecular bonds. Moreover, the Auger and Coster–Kronig electrons from the higher shells can be quite numerous. They are of such low energy that they travel only a fraction of a cell diameter. This must be taken into consideration when estimating cell damage from radiation. The effect of radiationless transitions is quite important for certain radioactive isotopes that are administered to a patient, particularly when they are bound to the cellular DNA. We will discuss them further in Chap. 17.

15.10 Energy Transfer from Photons to Electrons

The attenuation coefficient gives the rate at which photons interact and leave the primary beam as they pass through the material. If a beam of monoenergetic photons of energy $E = h\nu$ and particle fluence Φ passes through a thin layer dx of material, the number of particles per unit area that interact in the layer, $-d\Phi$, is proportional to the fluence and the attenuation coefficient: $-d\Phi = \Phi\mu_{\text{atten}}\,dx$. The energy fluence is $\Psi = h\nu\Phi$. The reduction of energy fluence of unscattered photons is $-d\Psi = -h\nu\,d\Phi$. For a thick absorber we can say that the number of unscattered photons and the energy carried by unscattered photons decay as

$$\Phi_{\text{unscatt}} = \Phi_0 e^{-\mu_{\text{atten}}x}, \qquad \Psi_{\text{unscatt}} = \Psi_0 e^{-\mu_{\text{atten}}x}. \quad (15.34)$$

The total energy flow is much more complicated. Every photon that interacts contributes to a pool of secondary photons of lower energy and to a pool of electrons and positrons. Figure 15.15 shows the processes by which energy can move between the photon pool and the electron–positron pool.

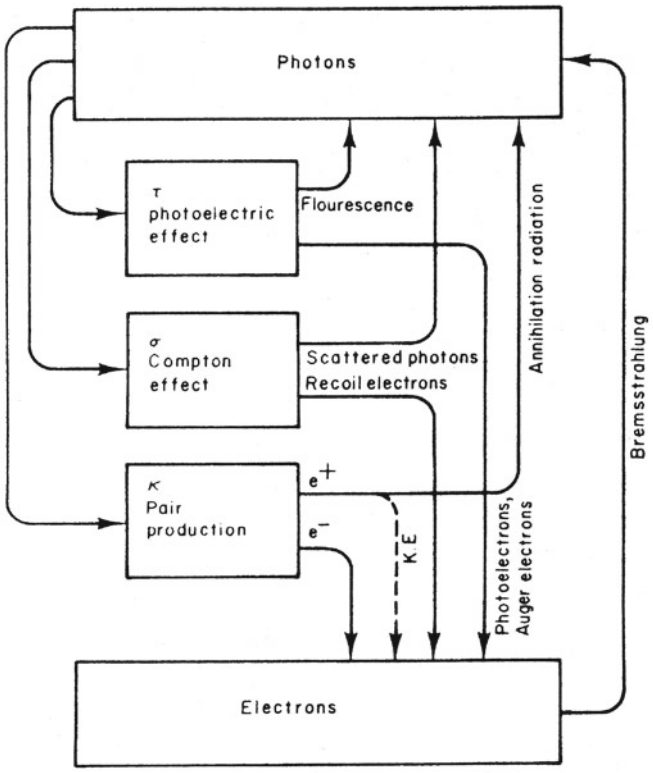

Fig. 15.15 Routes for the transfer of energy between photons and electrons. The four lines going to the lower box represent electrons; the others represent photons

Energy that remains as secondary photons, such as those resulting from fluorescence or Compton scattering, can travel long distances from the site of the initial interaction. Ionizing particles (photoelectrons, Auger electrons, Compton recoil electrons, and electron–positron pairs) usually lose their energy relatively close to where they were produced. We will see in Sect. 15.13 that for primary photons below 10 MeV, the mean free path of the secondary electrons is usually short compared to that of the photons. Damage to cells is caused by local ionization or excitation of atoms and molecules. This damage is done much more efficiently by the electrons than by the photons.

The *mass energy transfer coefficient* $\mu_{\rm tr}/\rho$ is a measure of the energy transferred from primary photons to charged particles in the interaction. If N monoenergetic photons of energy E strike a thin absorber of thickness dx, the amount of energy transferred to charged particles is defined to be

$$\overline{dE_{\rm tr}} = NE\,\mu_{\rm tr}\,dx,$$

so that

$$\frac{\mu_{\rm tr}}{\rho} = \frac{1}{\rho NE}\frac{\overline{dE_{\rm tr}}}{dx}. \tag{15.35}$$

We can relate $\mu_{\rm tr}$ to $\mu_{\rm atten}$. Suppose the material contains a single atomic species and that f_i is the average fraction of the photon energy that is transferred to charged particles in process i. (Different values of i denote the photoelectric effect, incoherent scattering, coherent scattering, and pair production.) Multiplying the number of photons that interact by their energy E and by f_i gives the energy transferred. Comparison with Eq. 15.23 shows that

$$\frac{\mu_{\rm tr}}{\rho} = \frac{N_A}{A}\sum_i f_i\sigma_i. \tag{15.36}$$

Coherent scattering produces no charged particles, so

$$\frac{\mu_{\rm tr}}{\rho} = \frac{N_A}{A}\left(\tau f_\tau + \sigma_{\rm incoh} f_C + \kappa f_\kappa\right). \tag{15.37}$$

Fraction f_τ for the photoelectric effect can be written in terms of δ, the average energy emitted as fluorescence radiation per photon absorbed. The quantity δ is calculated taking into account all atomic energy levels and the fluorescence yield for each shell. The average electron energy is $h\nu - \delta$, so

$$f_\tau = \frac{h\nu - \delta}{h\nu} = 1 - \frac{\delta}{h\nu}. \tag{15.38}$$

We can estimate δ by assuming that τ_K is the dominant term in the photoelectric cross section, Eq. 15.7. The probability that the hole in the K shell is filled by fluorescence is W_K. The energy of the photon is $B_K - B_L$ or $B_K - B_M$, and so on. A hole is left in a higher shell, which may decay by photon or Auger-electron emission. The latter is much more likely for the higher shells. Therefore, nearly all of the photons emitted have energy $B_K - B_L$, so we have the approximate relationship

$$\delta \approx W_K\,(B_K - B_L). \tag{15.39}$$

For Compton scattering, the fraction of the energy transferred to electrons is implicit in Eqs. 15.20 and 15.21. The transfer cross section $f_C\sigma_C$, is plotted in Fig. 15.7.

For pair production, energy in excess of $2m_ec^2$ becomes kinetic energy of the electron and positron. The fraction is

$$f_\kappa = 1 - \frac{2m_ec^2}{h\nu}. \tag{15.40}$$

All of these can be combined to estimate $\mu_{\rm tr}$.

We will see in Sect. 15.11 that charged particles traveling through material can radiate photons through a process known as *bremsstrahlung*. The *mass energy-absorption coefficient* $\mu_{\rm en}$ takes this additional effect into account. It is defined as

$$\frac{\mu_{\rm en}}{\rho} = \frac{\mu_{\rm tr}}{\rho}(1-g), \tag{15.41}$$

where g is the fraction of the energy of secondary electrons that is converted back into photons by bremsstrahlung in the

material. The fraction of the energy converted to photons depends on the energy of the electrons. Since the average electron energy is different in the three processes, we can write (again assuming noninteracting atoms in the target material)

$$\frac{\mu_{\text{en}}}{\rho} = \frac{N_A}{A} \sum_i f_i \sigma_i (1 - g_i). \tag{15.42}$$

In addition to bremsstrahlung, there is another process that converts charged-particle energy back into photon energy. Positrons usually come to rest and then combine with an electron to produce *annihilation radiation*. Occasionally, a positron annihilates while it is still in flight, thereby reducing the amount of positron kinetic energy that is available to excite atoms. While not mentioned in the International Commission on Radiation Units and Measurements (ICRU) Report 33 (1980) definition, this effect has been included in the tabulations of μ_{en}/ρ by Hubbell (1982). Seltzer (1993) reviews the calculation of μ_{tr}/ρ and μ_{en}/ρ.

The energy-transfer and energy-absorption coefficients differ appreciably when the kinetic energies of the secondary charged particles are comparable to their rest energies, particularly in high-Z materials. The ratio $\mu_{\text{en}}/\mu_{\text{tr}}$ for carbon falls from 1.00 when $h\nu = 0.5$ MeV to 0.96 when $h\nu = 10$ MeV. For lead at the same energies it is 0.97 and 0.74. Tables are given by Attix (1986). The difference between the attenuation and the energy-absorption coefficients is greatest at energies where Compton scattering predominates, since the scattered photon carries away a great deal of energy. Figure 15.16 compares μ_{atten}/ρ and μ_{en}/ρ for water.

Attenuation and energy-transfer coefficients are found in Hubbell and Seltzer (1996). These tables are also available on the web at http://www.nist.gov/pml/data/xraycoef/index.cfm . Another data source is a computer program provided by Boone and Chavez (1996).

We will return to these concepts in Sect. 15.15 to discuss the dose, or energy per unit mass deposited in tissue or a detector. First, we must discuss energy loss by charged particles.

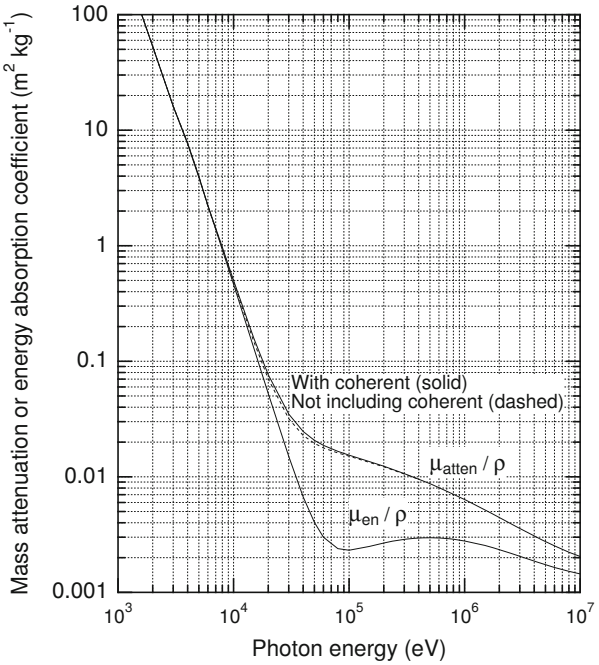

Fig. 15.16 Coherent and incoherent attenuation coefficients and the mass energy absorption coefficient for water. (Plotted from data in Hubbell 1982)

15.11 Charged-Particle Stopping Power

The behavior of a particle with charge ze and mass M_1 passing through material is very different from the behavior of a photon. When a photon interacts, it usually disappears: either being completely absorbed as in the photoelectric effect or pair production, or being replaced by a photon of different energy traveling in a different direction as in Compton scattering. The exception is coherent scattering, where a photon of the same energy travels in a different direction. A charged particle has a much larger interaction cross section than a photon—typically 10^4–10^5 times as large. Therefore the "unattenuated" charged-particle beam falls to zero almost immediately.

Each interaction usually causes only a slight decrease in the particle's energy, and it is convenient to follow the charged particle along its path. Figure 15.27 shows the tracks of some α particles (helium nuclei) in photographic emulsion. The spacing of the fiducial marks at the bottom is 10 μm. Each particle entered at the bottom of the figure and stopped near the top. Figures 15.28 and 15.29 show the tracks of electrons. Figure 15.28 is in photographic emulsion, while Fig. 15.29 is in water. We will be discussing these tracks in detail in Sect. 15.14. For now, we need only note that the α-particle tracks are fairly straight, with some deviation near the end of the track. The electrons, being lighter, show considerably more scattering.[3]

[3] This distinction between photons and charged particles represents two extremes on a continuum, and we must be careful not to adhere to the distinction too rigidly. A photon may be coherently scattered through a small angle with no loss of energy, while a charged particle may occasionally lose so much energy that it can no longer be followed.

It is convenient to speak of how much energy the charged particle loses per unit path length, the *stopping power*, and its *range*—roughly, the total distance it travels before losing all its energy. The stopping power is the expectation value of the amount of kinetic energy T lost by the projectile per unit path length. The term "power" is historical. The units of stopping power are J m^{-1} not J s^{-1}. The *mass stopping power* is the stopping power divided by the density of the stopping material and is analogous to the mass attenuation coefficient (often we will say stopping power when we actually mean mass stopping power):

$$S = -\frac{dT}{dx}, \qquad \frac{S}{\rho} = -\frac{1}{\rho}\frac{dT}{dx}. \tag{15.43}$$

In the energy-loss process, the projectile interacts with the target atom. The projectile loses energy W, which becomes kinetic energy or internal excitation energy of the atom. Internal excitation may include ionization of the atom. If the atoms in the material act independently, the cross section per atom for an interaction that results in an energy loss between W and $W + dW$ is $(d\sigma/dW)dW$. The results of Sect. 14.5 can be used to write the probability that a projectile loses an amount of energy between W and $W + dW$ while traversing a thickness dx of a substance of atomic mass number A and density ρ:

$$\text{(probability)} = \frac{\overline{n}}{N} = \frac{N_A \rho}{A}\, dx\, \frac{d\sigma}{dW}\, dW. \tag{15.44}$$

The average total energy loss is

$$dT = \frac{N_A \rho}{A} dx \int_0^{W_{\max}} W\, \frac{d\sigma}{dW}\, dW, \tag{15.45}$$

and the mass stopping power is

$$\frac{S}{\rho} = \frac{N_A}{A} \int_0^{W_{\max}} W\, \frac{d\sigma}{dW}\, dW. \tag{15.46}$$

The integral is sometimes called the *stopping cross section* ϵ. Its units are J m^2.

Figure 15.17 shows the mass stopping power for protons, α particles ($z = 2$, $M_\alpha = 4M_p$), and electrons and positrons ($z = \pm 1$) in carbon as a function of energy. We see a number of features of these curves:

1. All of the stopping power curves have roughly the same shape, rising with increasing energy, reaching a peak, and then falling. (The electron and positron curves peak at a lower energy than is shown in the figure.)
2. There is a region where the stopping power falls approximately as $1/T$.
3. At still higher energies the curves rise again. This can be seen for the electron and positron curves above 1 MeV. Similar increases occur in the proton and α-particle curves at higher energies than are plotted here.

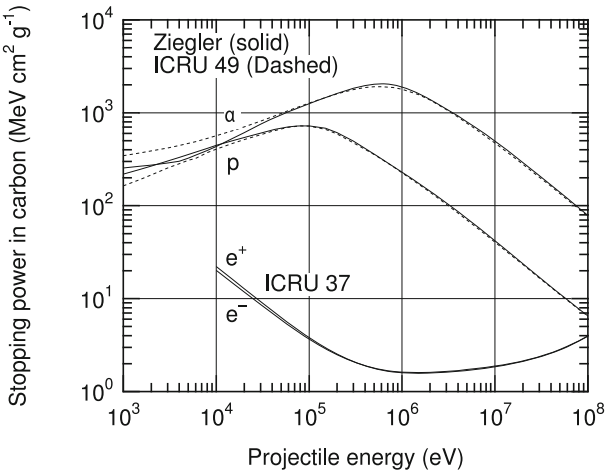

Fig. 15.17 The mass stopping power for electrons (e^-), positrons (e^+), protons (p), and α particles in carbon vs kinetic energy. Plotted from data in ICRU 37, ICRU 49, and the program SRIM (Stopping and Range of Ions in Matter), version 96.04 (see Ziegleret al. 1985)

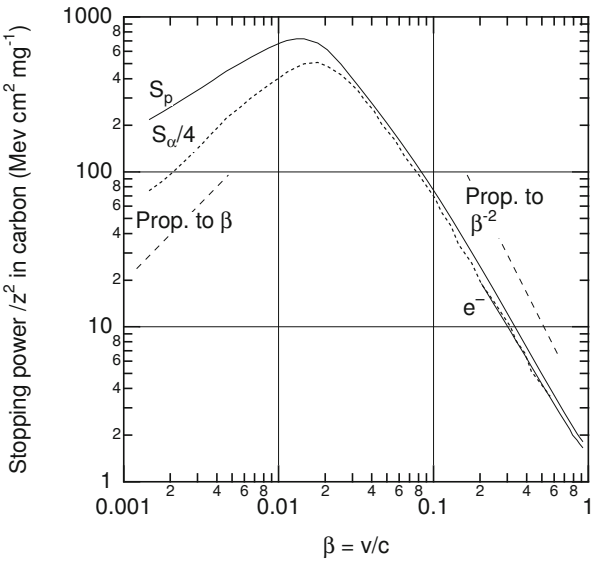

Fig. 15.18 The scaled stopping power. The stopping power in carbon is plotted vs the speed $\beta = v/c$ of the projectile for electrons, protons, and α particles. The α-particle stopping power has been divided by 4, the square of the particle charge z. Proton and α-particle stopping powers are from the program SRIM (see caption for Fig. 15.17). The electron stopping power is from ICRU Report 37 (1984)

The similarities suggest that the stopping power curves for different projectiles may be related. Figure 15.18 shows the similarities more clearly. The stopping powers are plotted vs particle speed in the form $\beta = v/c$. At low energies ($\beta \ll 1$) β is related to kinetic energy by

$$\beta = \left(\frac{2T}{Mc^2}\right)^{1/2}. \tag{15.47}$$

For larger values of β, the relativistically correct expression

$$\beta = \left[1 - \left(\frac{1}{T/Mc^2 + 1}\right)^2\right]^{1/2}, \tag{15.48}$$

was used to convert Fig. 15.17 to Fig. 15.18. The α-particle stopping power in Fig. 15.17 has been divided by the square of the α-particle charge number $z^2 = 4$. All three curves of $(1/z^2)S/\rho$ vs β are described by very similar functions for $\beta > 0.04$, though the electron and α-particle curves are about 10 % below the proton curve.[4] At low speeds the scaled α-particle curve falls significantly below the proton curve. The reason, the formation of an electron cloud on the α particle, is discussed below.

It is not difficult to understand the basic shape of the stopping power curve. Most of the energy loss is from the projectile to the electrons of the target atom. Since the electrons are bound to the target nucleus, the speed with which the projectile passes the target is important. Imagine pushing slowly on a swing with a force that gradually increases and then decreases. The net force on the swing is the vector sum of the external force exerted $\mathbf{F}_{\text{ext}}$, the vertical pull of gravity, and the tension in the ropes and equals the swing's mass times acceleration. For small horizontal displacements x from equilibrium, the vector sum of the weight and the tension in the string is horizontal and nearly proportional to x. It points toward the equilibrium position, and for small displacements is approximately a linear restoring force. If the proportionality constant is k, $ma = F_{\text{ext}} - kx$. This is the equation of motion for an undamped harmonic oscillator (Chap. 10 and Appendix F). If the force builds up slowly, there is a very small acceleration, and the swing angle changes so that $F_{\text{ext}} \approx kx$. As the force decreases the swing returns to its resting position. All of the work that was done to displace the swing is now returned as work by the swing on the source of the external force. No net energy has been imparted to the swing. This is called an *adiabatic* process or approximation, a slightly different use of the term than in Chap. 3.

At the other extreme, the force could be applied for a very short time, building up to a peak and falling quickly. In this case, the swing does not have time to move and $F_{\text{ext}} = ma$. This can be integrated to give

$$\int F_{\text{ext}}\, dt = m \int a\, dt = m(v_{\text{final}} - v_{\text{initial}}). \tag{15.49}$$

The swing acquires a velocity and hence some kinetic energy. The integral of force with respect to time is called the *impulse*, and this limit is the *impulse approximation*.

[4] A value $\beta = 0.04$ corresponds to a kinetic energy of 400 eV for electrons, 800 keV for protons, and 3.2 MeV for α particles.

The two limits depend on whether the duration of the force is long or short compared to the natural period of the swing. The atomic electrons are bound, and they have a natural period that is the circumference of their orbit divided by their speed v_{electron}. The length of time that a projectile exerts a force on the electrons is roughly the diameter of the atom divided by the projectile speed. Ignoring factors of 2π, we see that the passage of the projectile will be adiabatic if

$$\frac{d_{\text{atom}}}{v_{\text{projectile}}} \gg \frac{d_{\text{atom}}}{v_{\text{electron}}}$$

or $v_{\text{projectile}} \ll v_{\text{electron}}$. The impulse approximation will be valid if $v_{\text{projectile}} \gg v_{\text{electron}}$.

This is sufficient to explain the shape of the stopping-power curves in Fig. 15.18. When the projectile has very low energy it moves past the atom so slowly that the electrons have time to rearrange themselves[5] and then return to their original state as the projectile leaves, restoring to the projectile the energy that they received while rearranging. As the projectile speed increases, the process is no longer adiabatic, first for the more slowly moving outer electrons and then for more and more of the inner atomic electrons as the speed increases. At the other extreme, when the projectile speed becomes high enough, we can think of the process in terms of the impulse approximation. The faster the projectile moves by, the shorter the time the force is applied and the smaller the energy transfer. The energy transfer is most effective, and the peak of the stopping power occurs, when the speed of the projectile is about equal to the speed of the atomic electrons in the target.

The cross section $d\sigma/dW$ in Eqs. 15.44–15.46 is the sum of cross sections for three possible processes. We have already described the stopping power due to interactions of the projectile with the target electrons, S_e. There is another contribution to the stopping power from interactions of the projectile with the target nucleus, S_n. It is also possible for the energy loss to involve the radiation of a photon, so we also have radiative stopping power, S_r. Because these are independent processes, the total stopping power and the cross section are each the sum of three terms:

$$\begin{aligned} \frac{S}{\rho} &= \frac{S_e}{\rho} + \frac{S_n}{\rho} + \frac{S_r}{\rho}, \\ \frac{d\sigma}{dW} &= \left(\frac{d\sigma}{dW}\right)_e + \left(\frac{d\sigma}{dW}\right)_n + \left(\frac{d\sigma}{dW}\right)_r. \end{aligned} \tag{15.50}$$

To compare these processes, we need to consider the maximum energy that can be transferred, as well as the relative

[5] Classically, if the electrons go around the nucleus many times while the projectile moves by, the shape of their orbits can change in response to the projectile. Quantum mechanically, the shape of the wave function can change, but the quantum numbers do not change.

Table 15.3 Maximum energy transfer and relative importance of nuclear and radiative interactions for various projectiles and targets

Projectile	Target	Nuclear W_{max} (eV)	Electron W_{max} (eV)	S_n/S	S_r/S
Electron, 100 keV	Hydrogen	240	50,000		0.01 %
	Carbon	20	50,000		0.09 %
	Lead	1	50,000		2.2 %
Electron, 1 MeV	Hydrogen	4300	500,000		0.13%
	Carbon	360	500,000		0.65 %
	Lead	20	500,000		11.5 %
Proton, 10 keV	Hydrogen	5000	20	1.7 %	
	Carbon	2800	20	1.6 %	
	Lead	200	20	1.5 %	
Proton, 100 keV	Hydrogen	50,000	220	0.17 %	
	Carbon	28,400	220	0.15 %	
	Lead	1900	220	0.24 %	
Proton, 1 MeV	Hydrogen	500,000	2200	0.11 %	
	Carbon	280,000	2200	0.07 %	
	Lead	19,000	2200	0.09 %	
α particle, 10 keV	Hydrogen	6400	5	27 %	
	Carbon	7500	5	12 %	
	Lead	700	5	10 %	
α particle, 100 keV	Hydrogen	64,000	50	1.6 %	
	Carbon	75,000	50	1.1%	
	Lead	7400	50	1.8 %	
α particle, 1 MeV	Hydrogen	640,000	500	0.13 %	
	Carbon	750,000	500	0.12 %	
	Lead	74,000	500	0.20 %	

probability of each process. The maximum possible energy transfer W_{max} can be calculated using conservation of energy and momentum. For a collision of a projectile of mass M_1 and kinetic energy T with a target particle of mass M_2 which is initially at rest, a nonrelativistic calculation gives

$$W_{max} = \frac{4TM_1M_2}{(M_1 + M_2)^2}. \tag{15.51}$$

The analogous relativistic equation (needed, for example, when the projectile is an electron) is

$$W_{max} = \frac{2(2 + T/M_1c^2)TM_1M_2}{M_1^2 + 2(1 + T/M_1c^2)M_1M_2 + M_2^2}. \tag{15.52}$$

The values of W_{max} for representative projectiles and targets are shown in Table 15.3, along with the percentage of the stopping power due to nuclear collisions. For electrons, the table also shows the percentage of the stopping power due to radiative transitions. The percentages are calculated from ICRU Report 49 (1993). Electrons can scatter from nuclei, but the amount of recoil energy transferred to the nucleus is very small. Although electrons undergo a great deal of nuclear scattering, which results in a tortuous path through material, they lose very little energy in a nuclear scattering. The heavier projectiles can lose relatively more energy in each nuclear collision than in each electron collision. For a given kind of projectile, nuclear stopping is more important at lower energies, because less energy can be transferred to an electron. The heavier the projectile for a given energy, the more important the nuclear term becomes, for the same reason.

The collision of electrons with electrons is a special case. Equation 15.51 or 15.52 gives $W_{max} = T$. Consider the collision of two billiard balls of the same mass. If the projectile misses the target, it continues straight ahead with its original energy and $W = 0$. If it hits the target head on, it comes to rest and the target travels in the same direction with the same energy that the projectile had—a situation indistinguishable from the complete miss. It is customary (but arbitrary) in the case of identical particles to say that the particle with higher energy is the projectile, so $W_{max} = T/2$. This adjustment has been made in Table 15.3 for electrons on electrons and protons on protons.

Radiation is only important for electrons and occurs in a certain fraction of the elastic electron scatterings from the target nucleus. Nuclear scattering gives the electron a fairly large acceleration. Classically, an accelerated charged particle radiates electromagnetic waves. This process is called *bremsstrahlung*—braking or deceleration radiation. The energy radiated is proportional to the square of the acceleration, so bremsstrahlung is only important for light projectiles. There is also a contribution from electron–electron or positron–electron scattering. The electron–electron contribution vanishes at low energies, although the positron–electron

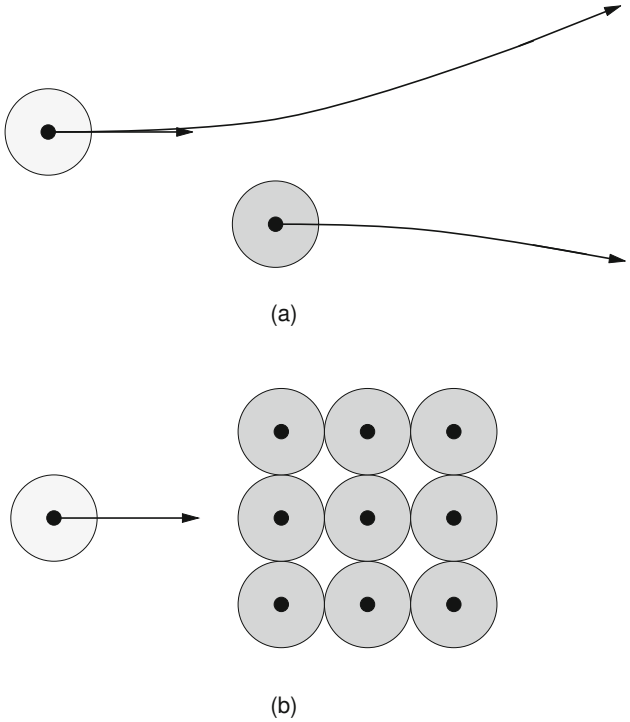

Fig. 15.19 A projectile, which may or may not carry an electron cloud, moves past a target atom. **a** In a gas the projectile interacts with one atom at a time. **b** In a liquid or a solid, neighboring atoms may influence the interaction

bremsstrahlung does not.[6] We will see in Chap. 16 that bremsstrahlung is an important component of the x-ray spectrum produced when a beam of electrons strikes a target. Even so, the fraction of the electron energy that is converted to radiation is small.

An atom has a radius of a few times 10^{-10} m. The nucleus of the atom is much smaller, about 10^{-15} m, and contains most of the atom's mass. The atom's size is determined by the electron cloud around the nucleus. Figure 15.19a shows a projectile entering at the left and traveling to the right through a gas. It interacts with one target atom at a time. The solid black dots represent the nuclei of the projectile and the target atom. The shaded circles represent the electron clouds. The projectile may or may not have an electron cloud, which is shown with lighter shading. Figure 15.19b shows the interaction with a solid or liquid in which the target atoms are tightly packed, and it may not be accurate to say that the projectile interacts with only one atom at a time.

[6] This difference can be understood classically. In the first approximation, the radiation by a charge is proportional to the product of the charge times its acceleration, qa. For two interacting electrons, $a_1 = -a_2$, $q_1 = q_2$, and the sum of these two terms vanishes. For an electron and a positron $a_1 = -a_2$, $q_1 = -q_2$, and the two terms add.

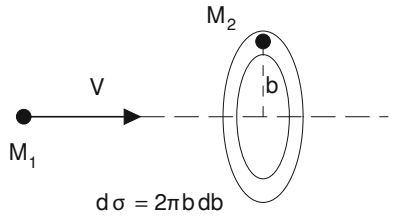

Fig. 15.20 The impact parameter is the perpendicular distance from the target particle to a line extended from the projectile in the direction of its velocity before the interaction

Classically, the motion of a charged projectile past a charged target depends on the charges and masses of the particles, the initial velocity or kinetic energy of the projectile, and the *impact parameter* b, which is the perpendicular distance from a line through the initial velocity of the projectile to the target, as shown in Fig. 15.20. The classical cross section for having an impact parameter between b and $b + db$ is the area of the ring, $2\pi b\, db$. If we could relate b to the energy loss W, we would have the cross section $d\sigma/dW$ of Eq. 15.46.

The energy-loss process is quite complicated, and the cross section cannot be calculated exactly. A great deal of experimental and theoretical work on stopping powers has been done, extending from 1899 to the present time. The history is nicely reviewed by Ziegler et al. (1985). Much of the recent work on stopping powers has been motivated by the use of ion implantation to make semiconductors, the analysis of materials using ion beams, and medical applications. Currently stopping powers of low-energy heavy ions can be calculated with an accuracy of better than 10 %. For high-speed light ions the accuracy is better than 2 %.

15.11.1 Interaction with Target Electrons

We first consider the interaction of the projectile with a target electron, which leads to the *electronic stopping power*, S_e. Many authors call it the *collision stopping power*, S_{col}. There can be interactions in which a single electron is ejected from a target atom or interactions with the electron cloud as a whole (a *plasmon* excitation). The stopping power at higher energies, where it is nearly proportional to β^{-2}, has been modeled by Bohr, by Bethe, and by Bloch (see the review by Ahlen 1980). The Bethe–Bloch model is also valid for relativistic energies. A nonrelativistic model for high energies was developed by J. Lindhard and his colleagues (see references in Ziegler et al. 1985). It allows more accurate calculations of which electrons in the target receive energy from the projectile.

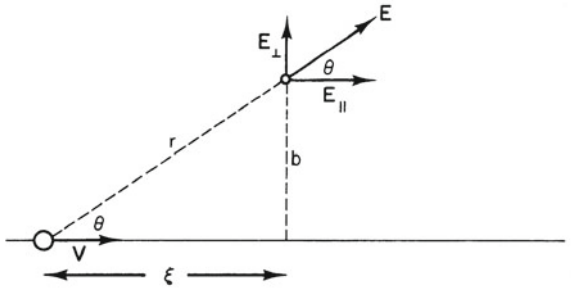

Fig. 15.21 A heavy particle of charge ze, mass M, and velocity $\mathbf{V}$ moves past a stationary electron

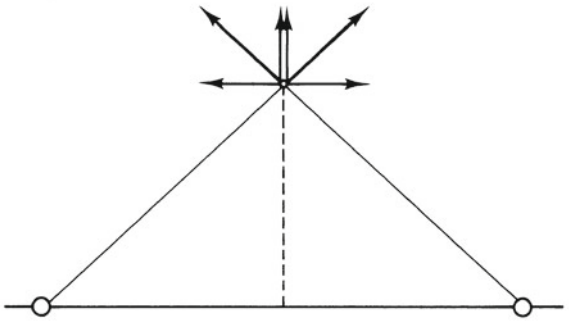

Fig. 15.22 Why the parallel component of $\mathbf{p}$ is zero. For every point where the projectile gives a particular $\mathbf{E}_\parallel$, there is a symmetric point where $\mathbf{E}_\parallel$ is equal but opposite. The components $\mathbf{E}_\perp$ are in the same direction in both places, so the perpendicular component of $\mathbf{p}$ does not vanish

We can gain considerable insight into the high-energy loss process by making a classical calculation of the cross section for transferring energy to an electron using the impulse approximation. This is a simplification of the Bethe–Bloch model. In our model, a heavy projectile passes by a free electron that is at rest. Momentum is transferred from the projectile to the electron. Because of its large mass, the projectile's velocity does not change appreciably, but the lighter electron acquires an appreciable velocity and kinetic energy. If the momentum transferred to the electron is $\mathbf{p}$, its kinetic energy is $p^2/2m_e$. That kinetic energy must have been lost by the projectile.

Figure 15.21 shows a particle of mass M, charge ze, and velocity $V = \beta c$ moving past a stationary electron. The impact parameter b is the perpendicular distance from the electron to the path of the projectile. The distance from the projectile to the electron is r, and the distance along the path to the point of closest approach is ξ. The momentum transferred to the electron is $\mathbf{p} = \int \mathbf{F}dt = -e\int \mathbf{E}dt$. By symmetry, there is no component of $\mathbf{p}$ parallel to the path of the projectile. The reason is shown in Fig. 15.22. For each location of the projectile that gives a parallel component of $\mathbf{F}$ in one direction, there is a position an equal distance on the other side of the point of closest approach that gives a component of $\mathbf{F}$ with the same magnitude but in the opposite direction. The perpendicular component of $\mathbf{F}$ is the same for both locations, so there is a net perpendicular component of momentum transfer. The magnitude of the perpendicular component of $\mathbf{E}$ is

$$E_\perp = E\sin\theta = \frac{ze\sin\theta}{4\pi\epsilon_0 r^2} = \frac{zeb}{4\pi\epsilon_0 r^3} = \frac{ze}{4\pi\epsilon_0}\frac{b}{\left(\xi^2+b^2\right)^{3/2}}.$$

The perpendicular impulse is

$$\int F_\perp dt = -e\int E_\perp (dt/d\xi)d\xi.$$

If the fraction of energy lost by the projectile is small, then $dt/d\xi = 1/\beta c$ does not change during the collision. The magnitude of the impulse is therefore

$$\begin{aligned} p &= -\frac{e}{V}\int E_\perp d\xi = -\frac{ze^2 b}{4\pi\epsilon_0\beta c}\int_{-\infty}^{\infty}\frac{d\xi}{(\xi^2+b^2)^{3/2}} \\ &= -\frac{ze^2 b}{4\pi\epsilon_0\beta c}\lim_{x\to\infty}\left[\frac{\xi}{b^2(\xi^2+b^2)^{1/2}}\right]_{-x}^{x} \\ &= -\frac{2ze^2}{4\pi\epsilon_0\beta c b}. \end{aligned}$$

The smaller the impact parameter, the greater the momentum transfer to the electron. The kinetic energy acquired by the electron is

$$W = \frac{p^2}{2m_e} = \frac{2z^2e^4}{(4\pi\epsilon_0)^2 m_e c^2\beta^2 b^2}.$$

The factor $e^4/(4\pi\epsilon_0)^2 m_e c^2$ depends only on the charge and mass of the electron. It can be written as $r_e^2 m_e c^2$, where r_e is the classical radius of the electron (Eq. 15.17). The factor has the numerical value

$$r_e^2 m_e c^2 = 6.50\times10^{-43}\,\mathrm{J\,m^2} = 4.06\times10^{24}\,\mathrm{eV\,m^2}.$$

Using this notation the energy transfer per target electron is

$$W = \frac{2z^2 r_e^2 m_e c^2}{\beta^2 b^2}. \tag{15.53}$$

Note that W does not depend on the mass of the heavy projectile, but only on its speed. As the speed becomes less, the energy transfer becomes greater, because the projectile takes longer to move past the electron and the force is exerted for a longer time (as long as the time is still short enough so that the impulse approximation remains valid).

If the electrons are uniformly distributed, the cross section for each electron is $d\sigma = (d\sigma/dW)dW = 2\pi b\,db$. This can be written, with the help of Eq. 15.53, in terms of W:

$$\frac{d\sigma}{dW}dW = \frac{4\pi z^2 r_e^2 m_e c^2}{2\beta^2}\frac{dW}{W^2}. \tag{15.54}$$

This expression diverges as W approaches zero, corresponding to very large impact parameters. However, the assumption that the target electrons are free fails in this limit, so that there is some effective lower limit $W_{\min}$. Also, the greater the impact parameter, the longer the electron will experience the force exerted by the projectile (though it will be weaker). If the time is too long, the electron can move in response to the force and not absorb as much energy; the impulse approximation is no longer valid. We have already seen that there is a maximum energy transfer $W_{\max}$. Multiplying the cross section by W, integrating from $W_{\min}$ to $W_{\max}$, and noting that there are Z electrons per target atom, we obtain

$$\frac{S_e}{\rho} = \frac{4\pi N_A r_e^2 m_e c^2}{\beta^2}\frac{Z}{A}z^2 \ln\left(\frac{W_{\max}}{W_{\min}}\right). \tag{15.55}$$

The factor $4\pi N_A r_e^2 m_e c^2$ has the value 30.707 eV m^2 mol^{-1} = 0.307 07 MeV cm^2 mol^{-1}.

A quantum-mechanical calculation gives a result of essentially the same form as Eq. 15.55. The logarithmic term includes both ionization and plasmon excitation[7] and is called the *stopping number per atomic electron* $L(\beta, z, Z)$:

$$\frac{S_e}{\rho} = \frac{4\pi r_e^2 m_e c^2}{\beta^2} N_A \frac{Z}{A} z^2 L(\beta, z, Z). \tag{15.56}$$

For heavy charged particles L has the form

$$L(\beta, z, Z) = L_0 + zL_1 + z^2 L_2,$$
$$L_0 = \ln\left(\frac{\beta^2}{1-\beta^2}\right) + \ln\left(\frac{2m_e c^2}{I(Z)}\right) - \beta^2 - \frac{C}{Z} - \frac{\delta}{2}. \tag{15.57}$$

Equation 15.56 with $L = L_0$ is often called the *Bethe–Bloch formula*. The second term in L_0 depends on $I(Z)$, the ionization potential of the atoms in the absorber, averaged over all the electrons in the atom. Values of $I(Z)$ have been calculated theoretically and also derived from measurements of the stopping power. They range from 14.8 eV for hydrogen to 884 eV for uranium. The value 14.8 eV is greater than the ground-state energy of hydrogen, 13.6 eV, because the ejected electron has some average kinetic energy. Published values of I can vary considerably, depending on whether the other correction terms are present. For example, values of I in the literature for hydrogen range from 11 to 20 eV. Discussions of values for I and the various terms in L can be found in ICRU Report 49 (1993), in Ahlen (1980), and in Attix (1986). The term $\delta/2$ corrects for the *density effect*. The calculation above assumed that the electron experienced the full electric field of the projectile. However, other electrons in the absorber move slightly, polarizing the absorber and reducing the field. This effect becomes important at high energies as the electric field is distorted by relativistic effects. It also depends on the density of the absorber. A small density effect persists in conductors even at low energies; however, it is usually incorporated into the value of $I(Z)$. For the projectile energies we are considering, the density effect is most important for electrons.

An alternative nonrelativistic treatment by Lindhard and colleagues allows the use of accurate atomic electron density distributions and also considers the effect of electrons in neighboring atoms.[8] In the Lindhard model the stopping power is

$$\frac{S_e}{\rho} = \frac{N_A}{A}\int z^2 I(V, \rho_e)\rho_e 4\pi r^2 dr, \tag{15.58}$$

where z is the projectile charge, I is the *stopping interaction strength* in J m^2 (more often in eV pm^2),[9] ρ_e is the electron density in the atom (in units of the electron charge), and $4\pi r^2 dr$ is the volume element. Integration of ρ_e over all volume gives Z, the atomic number of the target. Comparison of Eqs. 15.58 and 15.46 shows that the integral in Eq. 15.58 is the stopping cross section per target atom.

Figure 15.23 shows how the Lindhard model explains why the stopping power falls below the $1/\beta^2$ curve at lower projectile velocities. Each panel shows the electron density in copper, $4\pi r^2\rho_e$, and the interaction strength I. Their product, the solid line, is the integrand in Eq. 15.58. The integral is taken from 0 to 0.14 nm [1.4 Å (angstrom)]. The K, L, and M shells of copper can be seen in the electron density curve. Figure 15.23a is for a 10-MeV proton or some other heavy ion with the same speed. The projectile is moving fast enough so that all electrons except those in the K shell interact with it. Contrast this with Fig. 15.23b, which is for a 100-keV proton. The projectile speed is much less, and the interaction is almost exclusively with the outer electrons.[10]

[7] A plasmon excitation is due to the interaction of the projectile with the entire electron cloud of the atom.

[8] The electron density functions are calculated using quantum mechanics. The problem is to find the electron distribution by solving Schrödinger's equation with the potential distribution due to the nucleus and the potential due to the electron charge distribution for which one is solving. This self-consistent computation is called the *Hartree–Fock approximation*.

[9] I is not the same as the average ionization energy of Eq. 15.57.

[10] The solid line representing the integrand does not fall to zero at 0.12 nm = 1.2 Å because of the effect of electrons from neighboring atoms. In a solid there are no regions where the electron density is zero.

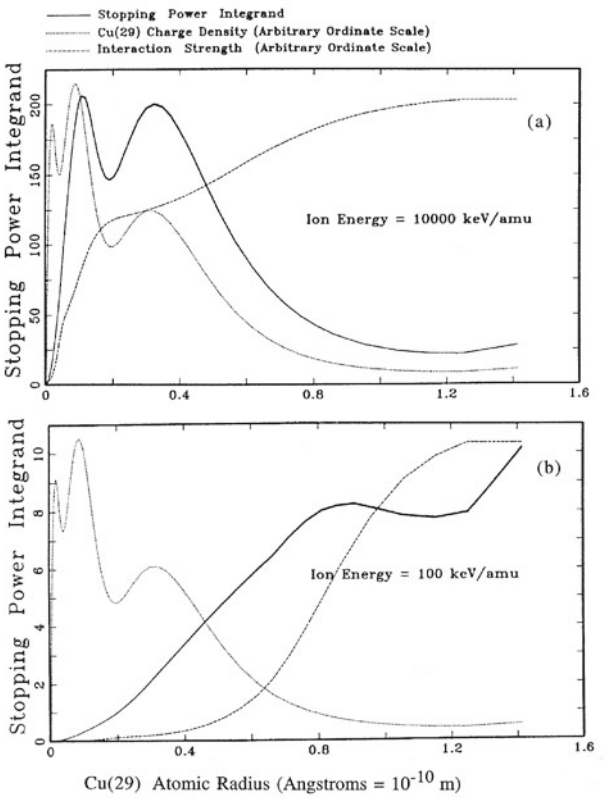

Fig. 15.23 Calculation of the stopping power at low energies involves integrating the product of the electron charge distribution in the target atom and the interaction strength function, which depends on the projectile speed. The *dotted line* shows the electron charge density for copper. The *solid line* shows the integrand. **a** For 10-MeV protons, all electrons but those in the K shell contribute. **b** For 100-keV protons the interaction function has changed, and only the outermost electrons contribute. Note the much different ordinate scales in **a** and **b**. (Provided by J. F. Ziegler)

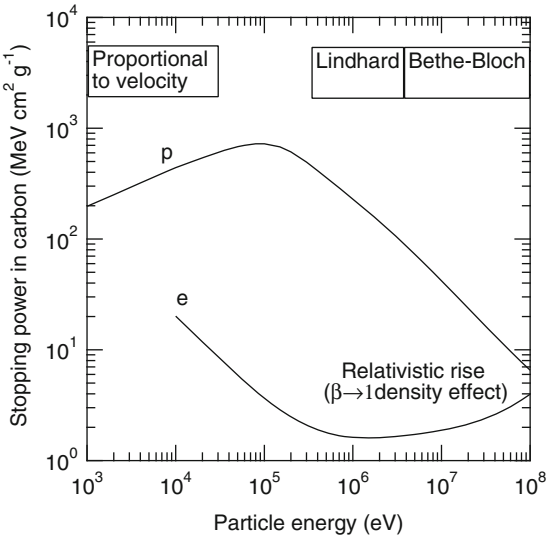

Fig. 15.24 Proton and electron stopping power vs energy in carbon, showing the regions in which various models are valid

Both the Bethe–Bloch and Lindhard models fail at low energy, because the electrons are not free and many of the interactions are adiabatic. Some models reviewed by Ziegler et al. (1985) predict a stopping power proportional to projectile velocity. This has been found to be true in general, though not for all elements. The experiments are quite difficult because of the thinness of the targets, contamination, etc. Figure 15.24 shows the regions where the various models apply for protons. For electrons, relativistic effects are important above about 500 keV. The rise in stopping power at high energies is due to the density effect (polarization of the electrons).

Another important effect at low energies is that the slowly moving ion can capture electrons, decreasing the value of z^2. Ziegler et al. (1985) discuss the scaling of data for different projectiles and the appropriate effective charge values. The average projectile charge follows a universal curve when plotted as a function of the appropriate combination of the speeds of the projectile and target electrons. They, and the ICRU Report 49 (1993), assume that for protons the effective charge is always unity. The theoretical justification is that the radius of the electron orbit in hydrogen is larger than the interatomic separation in solids.

15.11.2 Scattering from the Nucleus

The projectile can also scatter from the target atom as a whole. The recoil kinetic energy of the atom is lost by the projectile. Since the nucleus contains most of the mass, the kinematics are those of the bare projectile and the target nucleus, and this process is called *nuclear scattering*, with stopping power S_n. (Sometimes it is called *elastic scattering*, with a subscript that can cause it to be confused with electron interactions.)

Just as with Compton scattering, knowing the angle through which the projectile is scattered defines the amount of energy transferred to the target. The angle depends on the impact parameter. The problem can be solved for a given impact parameter if the force between the projectile and target is a function only of their separation and one knows the potential energy of their separation. The details are found in Ziegler et al. (1985). We will simply comment on the contributions to the potential energy. They are

1. The Coulomb force between the projectile and the target nucleus.
2. The Coulomb force between the projectile and the electron cloud of the target atom.
3. The Coulomb attraction between the target nucleus and any electrons surrounding the projectile.

4. The Coulomb repulsion between the electron clouds of the target and the projectile.
5. A term due to the Pauli exclusion principle if the projectile is an ion with an electron cloud. To see how it arises, suppose that both the projectile and target have both of their possible K-shell electrons. If the nuclei get close enough, they effectively form a single nucleus that cannot have four K-shell electrons. Therefore two of the electrons have to move to unfilled shells. This requires energy that comes from the kinetic energy of the projectile. This is called *Pauli promotion*. Even though the electrons have time to return to their original orbits for a slow projectile, the effect changes the overall potential and hence the projectile orbit and the probability of a particular energy transfer.
6. An *exchange term* that also arises from the Pauli principle, related to whether the spins of the projectile and target electrons are parallel or antiparallel.

Because nuclear scattering is relatively unimportant for the charged particles we are considering and because it does not lead to ionization, we will not describe any details of the calculations.

15.11.3 Stopping of Electrons

Equations similar to Eq. 15.56 are obtained for electrons and positrons. Recall that energy loss in nuclear scattering is negligible for positrons and electrons because they are so light, and that bremsstrahlung transfers some of the electron kinetic energy to radiation. Electrons and positrons are assumed to collect no screening charge. Even at low energies, the electron velocities are high enough so that the Bethe–Bloch model is used. The collision stopping power for electrons is[11]

$$\frac{S_e}{\rho} = 4\pi N_A r_e^2 m_e c^2 \frac{1}{\beta^2}\frac{Z}{A} L_{\pm}. \tag{15.59}$$

The subscript $\pm$ indicates that stopping number per electron is slightly different for electrons and for positrons. The exact forms can be found in Attix (1986) or in ICRU Report 37 (1984). In both cases L depends on $I(Z)$ and the density effect. An accurate calculation of the shell correction for electrons has not been made; therefore ICRU Report 37 omits the shell correction from the tables for electrons and positrons. This omission makes the use of Eq. 15.58 less accurate for electrons below 10 keV. The best values of S_e/ρ for electrons and positrons are obtained from theoretical calculations using Eq. 15.59 and values of $I(Z)$ determined from proton data.

[11] The literature often replaces the 4π by 2π for electrons and makes L twice as large.

15.11.4 Compounds

In dealing with compounds, it is frequently assumed that each atom in the target interacts independently with the projectile, as we assumed for photons. The stopping power per molecule is then equal to the sum of the stopping powers for each atom in the molecule. This leads to a formula analogous to Eq. 15.31, known as the *Bragg rule*:

$$\frac{S}{\rho} = \sum_i w_i \left(\frac{S}{\rho}\right)_i. \tag{15.60}$$

This equation applies to the collision, radiative, nuclear, and total stopping powers. The approximation is quite inaccurate near the peak of the stopping power curve, where the errors can be greater than a factor of 2. This is not surprising, given the behavior of the scattering function I in Fig. 15.23b. Most of the energy loss is to outer electrons—the conduction electrons if the substance is a metal.

In a semiconductor there are gaps in the energy levels, and this precludes the low-energy transfers. As a result, the stopping power is lower in semiconductors. In crystals, channeling can occur: the stopping power depends on the orientation of the trajectory with the crystal symmetry axis.

Carbon poses a particular problem. It is an important element in the body, and it has chemical bonds that range from metallic to insulating in nature. Various investigators have shown variations in stopping power of 30 % for ions in pure carbon, depending on how it was fabricated. Graphite can be made with different electrical conductivities, and there are associated differences in stopping power. Ziegler and Manoyan (1988) have applied charge-scaling techniques to several organic carbon compounds by considering separately the stopping due to closed atomic shells (cores) and the remaining bonds between different pairs of atoms.

ICRU Reports 37 (1984) and 49 (1993) handle departures from the Bragg rule in the first approximation by using different values of I for electrons in compounds. The density effect is important for electrons and also does not follow the Bragg rule.

Stopping-power values are found in ICRU Report 37 for positrons and electrons. ICRU Report 49 has stopping powers for protons and α particles. These data are also found on the web: http://www.nist.gov/pml/data/star/index.cfm. A computer program for protons and ions, SRIM (Stopping and Range of Ions in Matter) is described by Ziegler et al. (1985) and is available at www.srim.org. It is updated every few years.

15.12 Linear Energy Transfer and Restricted Collision Stopping Power

In modeling the effect of ionizing radiation on targets, whether they be radiation detectors, photographic emulsions, cells, or parts of cells, one often wants to know how much of a charged particle's energy is absorbed "locally," that is, within some region around a particle's trajectory. An accurate calculation is difficult, since some of the electrons produced may leave the region of interest. Also, the energy absorbed in some region of interest around a particle track comes both from energy lost by the particle while traversing that track segment and also from photons and charged particles produced elsewhere by the projectile. (This is discussed in detail in ICRU Report 16 1970.)

An approximation to the desired quantity is the *linear energy transfer* (LET) or the *restricted linear collision stopping power* L_Δ. It is defined as the ratio dT/dx, where dx is the distance traveled by the particle and dT is the mean energy loss to electrons that results in energy transfers less than some specified Δ. This use of the symbol L should not be confused with the stopping number of Eqs. 15.56–15.59. The quantity L_Δ can be calculated by replacing $W_{\max}$ by Δ in the expression for the stopping power. The value of Δ is usually specified in electron volts.

The electron stopping power S_e is numerically equal to L_∞. However, S_e is defined in terms of the energy *lost by the particle*, while L_∞ is defined in terms of energy *imparted to the medium*.

Note that although the quantity actually of interest may be the energy imparted within some region around the trajectory, this definition is based on energy transfers less than Δ. A quantity based on the region of interest would be easier to measure; L_Δ is easier to calculate.

ICRU Report 37 calculates L_Δ for positrons and electrons for values of Δ down to 1 keV. The report points out that such calculations are inaccurate for smaller values of Δ, even in light elements. ICRU Report 16 provides values of L_Δ for protons and heavy ions.

15.13 Range, Straggling, and Radiation Yield

We can see in Fig. 15.27 that the α particles, entering from the bottom with the same energy, all travel about the same distance before coming to rest. This distance is called the *range* of the α particles. It will be defined more precisely below.

We can estimate the range in the following way. The stopping power represents an average energy loss per unit path length. The actual energy loss fluctuates about the mean values given by the stopping power. If these fluctuations are neglected and the projectiles are assumed to lose energy continuously along their tracks at a rate equal to the stopping power, then one is making the *continuous-slowing-down approximation* (CSDA). In this approximation one can calculate the range, the distance a particle with initial energy T_0 travels before coming to rest or reaching some final kinetic energy T_f. A factor ρ is introduced to express the range in mass per unit area:

$$R_{\mathrm{CSDA}}(T_0, T_f) = \rho \int dx = \rho \int_{T_f}^{T_0} \frac{dT}{S_e + S_n + S_r}. \tag{15.61}$$

ICRU Report 37 (1984) discusses the problem of carrying the integration to $T_f = 0$.

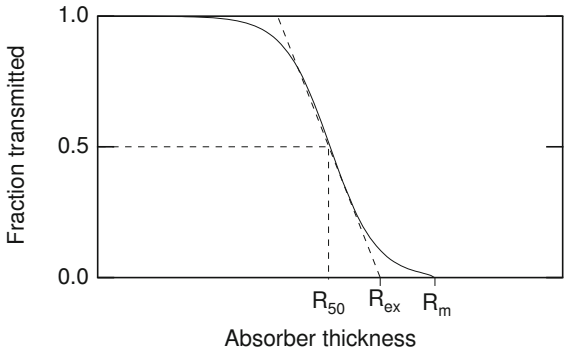

Fig. 15.25 Plot of the number of particles passing through an absorber vs its thickness to show the definition of various ranges. R_{50} is the median range, R_{ex} is the extrapolated range, and R_m is the maximum range

The CSDA range is not directly measurable. Measurements of the fraction $F(R)$ of monoenergetic particles in a beam that passes through an absorber of thickness R gives a curve like that of Fig. 15.25. Various ranges can be defined using this curve. The most easily measured is the median range R_{50}, corresponding to an absorber thickness that transmits 50 % of the incident particles. The extrapolated range R_{ex} is obtained by extrapolating the linear portion of the curve to the abscissa. The maximum range R_m is the thickness that just stops all of the particles; it is, of course, very difficult to measure. If $F(R)$ is known accurately one can define a *mean range* $\overline{R} = \int R(-dF/dR)dR / \int(-dF/dR)dR$. If the shape of the transmission curve is perfectly symmetrical about the mean, then R_{50} is equal to $\overline{R}$, even though they are conceptually quite different. For heavy projectiles $\overline{R}$ (usually approximated by R_{50}) provides the best estimate of R_{CSDA}.

The fluctuations in the range are called *straggling*. The straggling distribution has also been calculated. The track of a heavy projectile such as an α particle is fairly straight, because the various scattering interactions result only in small

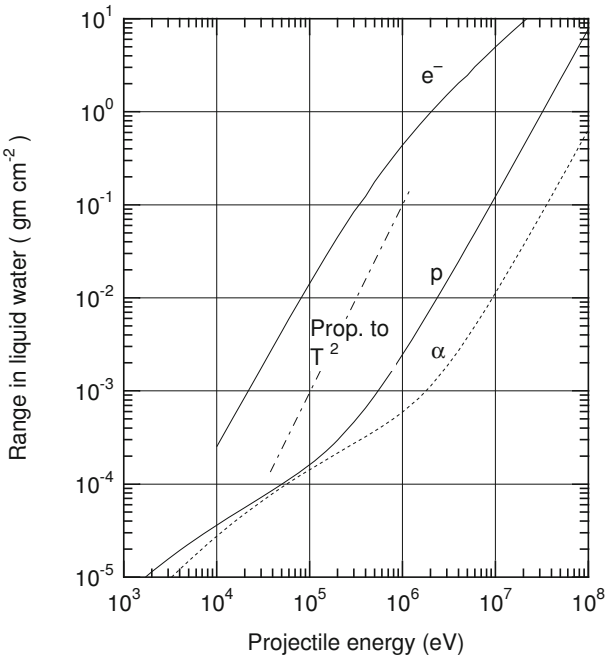

Fig. 15.26 Range of electrons, protons, and α particles in liquid water. Data are from ICRU Reports 37 (1984) and 49 (1993). Note that for water the range in gm cm^{-2} is the same as the range in cm

Fig. 15.27 Tracks of 22-MeV α particles in photographic emulsion. The α particles enter at the *bottom of the page* and come to rest near the top. The *small square fiducial marks* at the bottom are 10 μm apart. The features of the tracks are discussed in the text. (From Powell et al. 1959). Reproduced by permission of Prof. D. H. Perkins

angular deviations. The straggling results primarily from the fact that Sdx represents only an average energy loss in path length dx. The fluctuations can be integrated to give the spread in range; see Ahlen (1980) or ICRU Report 37 (1984) or ICRU Report 49 (1993) or the computer program SRIM (Ziegler et al. 1985).

Electrons and positrons are so light that they undergo large-angle scattering (occasionally from an electron, more often from an atomic nucleus). The resulting electron trajectories are quite tortuous, as can be seen in Figs. 15.28 and 15.29. The median or mean range for an electron is considerably less than R_{CSDA}. For electrons and positrons the extrapolated range R_{ex} corresponds most closely to R_{CSDA}, at least in materials with atomic number up to silver (Tung et al. 1979). Figure 15.26 shows ranges in water. At medium energies the dependence on energy is approximately T^2.

Tables of ranges are found in the references cited above or at the NIST web site http://www.nist.gov/pml/data/star/index.cfm.

The *radiation yield*, Y, is the fraction of the initial particle (usually electron) kinetic energy T_0 that is converted to bremsstrahlung photons as the electron comes to rest in the medium in question. The yield is calculated using the continuous-slowing-down approximation as (neglecting S_n)

$$Y(T_0) = \frac{1}{T_0}\int_0^{T_0} \frac{S_r(T)dT}{S_e(T) + S_r(T)}. \qquad (15.62)$$

15.14 Track Structure

We can gain insight into the interaction processes by examining tracks in photographic emulsions or in cloud chambers. Figures 15.27 and 15.28 are taken from a classic atlas of tracks in nuclear emulsions (Powell et al. 1959). They show the difference between the interaction of heavy and light particles in matter. Figure 15.27 shows the tracks of four cosmic-ray α particles, each of which entered the bottom of the figure and stopped near the top. The fiduciary marks along the bottom are 10 μm apart. Each track is about 195 μm long, corresponding to an initial α-particle energy of about 22 MeV. The emulsion has a density of 3.6×10^3 kg m^{-3}. Each black dot is a sensitive silver halide grain about 0.6 μm in diameter. At the beginning of the track, S is about 70 keV μm^{-1} or 42 keV per grain; 10 μm from the end of the track it is 200 keV μm^{-1} or 120 keV per grain. The energy that must be deposited in a grain to render it developable is about 2.8 keV. The amount of energy

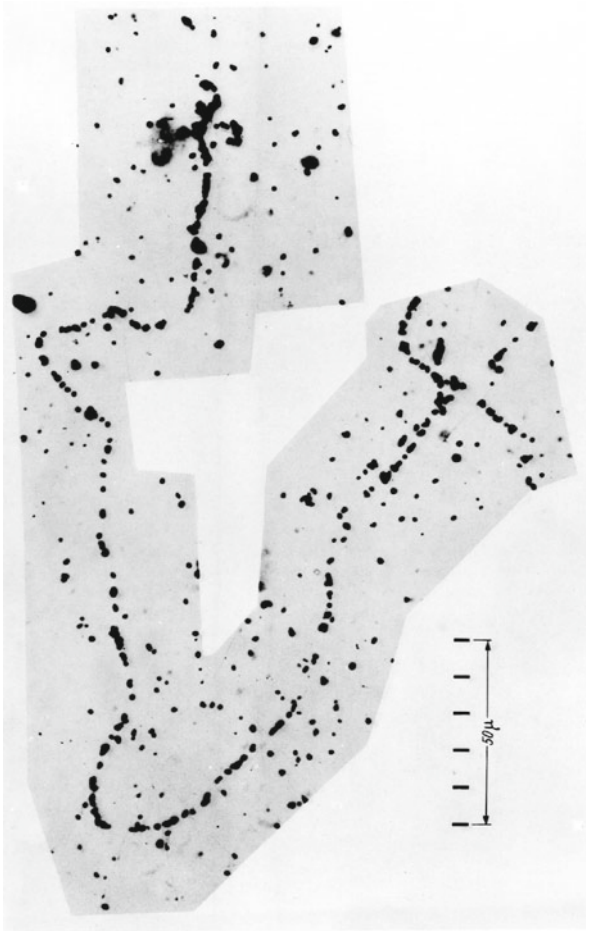

Fig. 15.28 Tracks of electrons in emulsion. An electron–positron pair was produced in the lower left corner. Each particle has an energy of about 250 keV. The details are discussed in the text. (From Powell et al. 1959. Reproduced by permission of Professor D. H. Perkins)

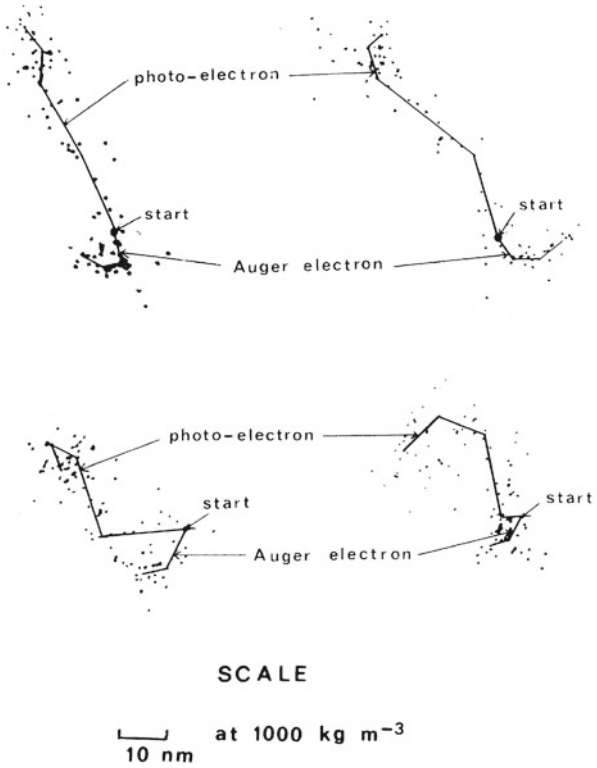

Fig. 15.29 Tracks of ≈1 keV electrons in a cloud chamber. An equivalent scale in water or tissue has been added. Photoelectrons and Auger electrons can be seen. The lines were drawn to guide the eye. (From Budd and Marshall 1983, pp. 19–32. Reproduced by permission of the Radiation Research Society)

deposited in each grain is so much larger than this that the track density is uniform. Small bumps of 1–4 grains can be seen occasionally along each track. Some of these are due to δ *rays*: electrons that have received enough energy to travel a few micrometers in the emulsion. Others are artifacts due to the general background fog. Multiple small-angle scattering causes small deviations in each track, which become greater as the α particle slows down.

In Figure 15.28 an electron–positron pair has been produced in the lower left corner of the emulsion by a 1.5-MeV photon. Each particle has a kinetic energy of about 250 keV. One immediately notices the tortuous path of both particles due to large-angle scattering. The stopping power near the beginning of the track is about 0.8 keV μm^{-1}, so that about 0.5 keV is deposited in each grain. About 30 μm from the end, the stopping power and the average amount of energy deposited in each grain are about 3 times larger. The upper track is considerably more dense near the end of its path. The failure of the other track to show this density increase could be due to annihilation of the positron in flight or to a large-angle scattering out of the emulsion.

Figure 15.29 shows the ionization produced by an electron at a much different scale. It was produced from a cloud chamber photograph of electron tracks in a low-density gas (Budd and Marshall 1983). The scale shows distances in liquid water or tissue that correspond to the same value of ρx, corrected for phase effects. Note that the scale shows 10 *nanometers*. An atomic diameter is 0.2–0.6 nm. In each case a photoelectron of energy between 950 and 1480 eV has been ejected from a gas atom in the cloud chamber. Auger electrons are also seen.

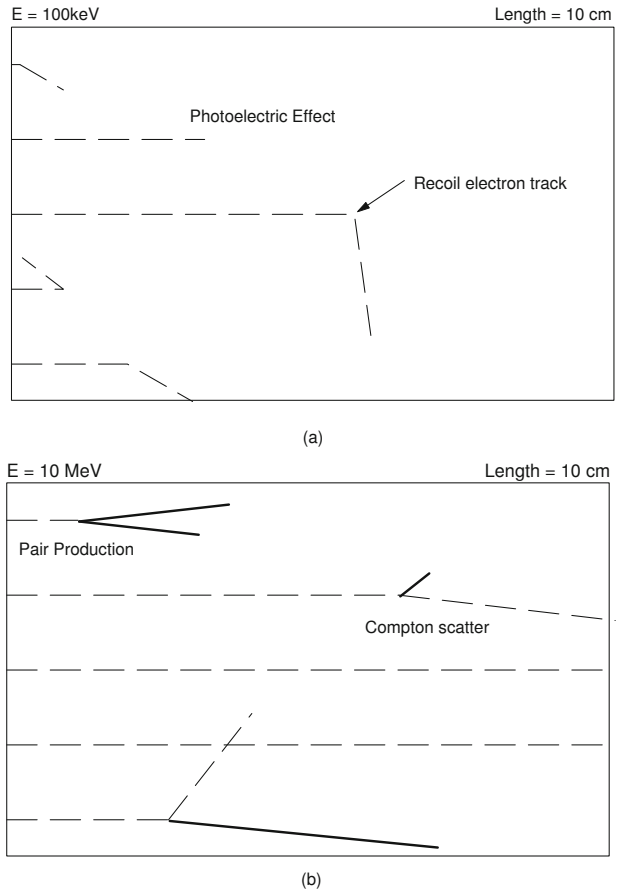

Fig. 15.30 A simulation of photons passing through a layer of water 10 cm thick. **a** The photon energy is 100 keV. One photon has a photoelectric interaction. The other four are Compton scattered. **b** The photon energy is 10 MeV. Two photons do not interact, one produces an electron–positron pair, and two Compton scatter

15.15 Energy Transferred and Energy Imparted; Kerma and Absorbed Dose

The response of a substance to radiation, whether it is the darkening of a photographic film, an electrical pulse in an ionization chamber, or the response of a tumor to radiation therapy, is due, directly or indirectly, to the ionization produced by charged particles that lose their kinetic energy in the substance through the stopping mechanisms we have just discussed. We now define some quantities that are used to describe the transfer of energy from photons to charged particles and the energy lost by charged particles due to ionization.

15.15.1 An Example

Before discussing the formal definition of these quantities, let us consider some examples of energy transfer by photons. Figure 15.30 shows some schematic interactions of photons in a sample of water 10 cm thick. They are drawn to scale.[12] In Fig. 15.30a five photons of energy 100 keV enter from the left. Photon tracks are dashed. One photon is absorbed by the photoelectric effect, and four are Compton scattered. The energy of the photoelectron and the Compton-scattered electrons is so low that the ranges are insignificant on this scale. In Fig. 15.30b the incident photons have 10 MeV energy. One has undergone pair production, two have Compton scattered, and two have passed through without interacting. The electron tracks are shown as thick solid lines. Their lengths are equal to the CSDA range of electrons or positrons of that energy. They are drawn as straight lines, even though the real tracks are tortuous.

One of the quantities of interest is the *energy transferred* to kinetic energy of charged particles in some mass of material. (We saw this briefly in the discussion surrounding Eq. 15.35.) Another is the *energy imparted* in some mass of material, which is the kinetic energy lost by charged particles as they come to rest. Figure 15.31 shows the distinction between the two quantities. It shows two photons from Fig. 15.30b: one that underwent pair production, and one that was Compton scattered. The water has been divided into ten slices, each 1 cm thick. No energy is transferred in the first slice. Energy is transferred by pair production in the second slice and by Compton scattering in the third slice. In each case the electron (or positron) produced loses kinetic energy in that slice and also in other slices. There is energy imparted in slices 2–8, even though the energy is transferred only in slices 2 and 3.

Consider now the actual numbers. In keeping with the literature,[13] we will call the energy transferred E_{tr}, even though we have been using T for kinetic energy. For pair production the energy transferred is

$$E_{\mathrm{tr}} = T_+ + T_- = h\nu_0 - 2m_e c^2$$
$$= 10 - 2 \times 0.511 = 8.978 \approx 9.0\,\mathrm{MeV}. \qquad (15.63)$$

The partition of energy between the electron and positron is stochastic. We assume for this example that about 60 % (5.4 MeV) goes to one member of the positron–electron pair and 40 % (3.6 MeV) to the other. These numbers are shown at the vertex of Fig. 15.31. From these energies the ranges can be determined. Measuring the distance from the end of the track to the boundary between each slice allows us to

[12] These examples were constructed with a pedagogical simulation program called MacDose (Hobbie 1992). The program is available at the book web site: www.oakland.edu/~roth/hobbie.htm. It runs on a Macintosh using OS-9 or earlier. There is also a 26-min video using MacDose that shows the concepts here in more detail (Hobbie 2009). It is free and available through iTunes. A more realistic but easily understood Monte Carlo simulation is described by Arqueros and Montesinos (2003).

[13] See ICRU Report 33 (1980) or Attix (1986).

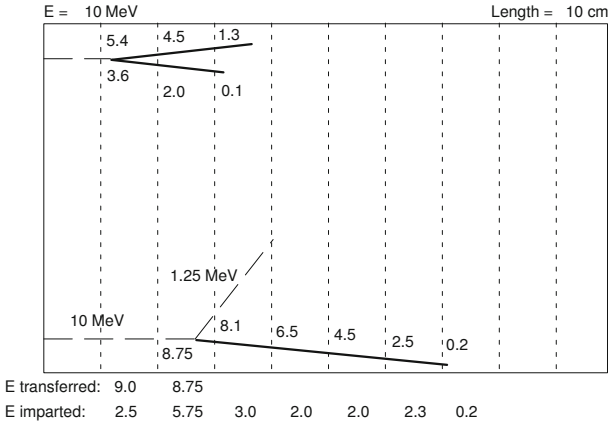

Fig. 15.31 The difference between energy transferred and energy imparted. Two of the photons from Fig. 15.30b are shown. The water has been divided into ten 1-cm slices. The numbers on the drawing show the charged-particle energy at the entrance to each slice. The energy transferred and the energy imparted in each slice are shown at the bottom

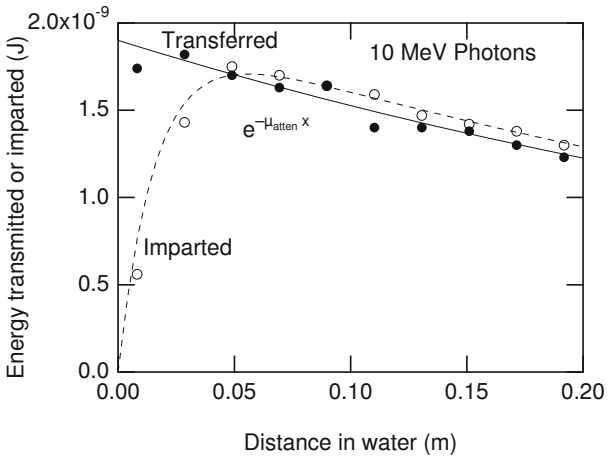

Fig. 15.32 Plot of energy transferred and energy imparted for a simulation using 40,000 photons of energy 10 MeV. The filled circles are the energy transferred in each slice, and the open circles are the energy imparted in each slice

determine the energy of each charged particle as it enters the slice. For the Compton scattering, 8.75 MeV is transferred to the recoil electron and the scattered photon has 1.25 MeV. The energy imparted by the 5.4-MeV particle is $5.4 - 4.5 = 0.9$ MeV in slice 2, $4.5 - 1.3 = 3.2$ MeV in slice 3, and 1.3 MeV in slice 4. Similar calculations can be done for the other charged particles. The energy transferred and the energy imparted in each slice are shown at the bottom of Fig. 15.31. This ignores any interaction of the 1.25-MeV Compton-scattered photon and assumes it leaves the volume of interest. Because for the 100-keV photons the range of the charged particles is small compared to 1 cm, the energy transferred and the energy imparted in each slice are the same in Fig. 15.30a.

Figure 15.32 shows a plot of the transferred and imparted energy for a uniform beam of 10-MeV photons all traveling to the right and striking a slab of water 20 cm thick. Both the energy transferred and the energy imparted are stochastic quantities. This simulation was done for 40,000 photons, and you can see the scatter in the points. The energy transferred falls exponentially as $\exp(-\mu_{\text{atten}} x)$.

15.15.2 Energy Transferred and Kerma

We found the energy transferred by calculating the energy of each electron or positron produced. The standard definition uses slightly different bookkeeping. It subtracts the energy of the photons leaving the volume of interest from those entering, and adds a term Q for the energy going into the volume due to changes in rest mass. For example, this is the $2m_e c^2$ of Eq. 15.63. The standard definition is

$$E_{\text{tr}} = (R_{\text{in}})_u - (R_{\text{out}})_u^{\text{nonr}} + Q. \tag{15.64}$$

The quantity R is radiant energy: the energy of particles (including photons) but not including rest energy. The subscript u means that it is the radiant energy of uncharged particles. The uncharged particles can be photons or neutrons.[14] Later we will use subscript c to denote the radiant energy of charged particles. The superscript "nonr" means that the quantity does not include radiant energy arising from bremsstrahlung or positron annihilation in flight from charged particles within the volume. The Q term is positive if mass is converted to energy (as in annihilation radiation) and negative if energy is converted to mass (as in pair production).

Using this method of calculating for Fig. 15.31 gives

$$E_{\text{tr}} = (R_{\text{in}})_u - (R_{\text{out}})_u^{\text{nonr}} + \sum Q = 10 - 0 - 2 \times 0.511 = 9.0\,\text{MeV}$$

for slice 2. For the third slice the equation gives

$$E_{\text{tr}} = (R_{\text{in}})_u - (R_{\text{out}})_u^{\text{nonr}} + \sum Q = 10 - 1.25 + 0 = 8.75\,\text{MeV}.$$

For the fourth slice, the uncharged radiant energy in is equal to the uncharged radiant energy out. In the fifth slice, if

[14] Neutrinos, which we will discuss in Chap. 17, travel such long distances without interacting that they are not considered in the calculations. Energy carried by neutrinos, which come from nuclear β decay, is assumed to have left the body.

the 1.25-MeV photon actually interacts as it appears to, we would have to include its energy transfer. In all the other slices the energy transferred is zero.

The energy transferred is a stochastic quantity, and so is the energy transferred per unit mass, dE_{tr}/dm. Its expectation value is the *kerma* (*k*inetic *e*nergy *r*eleased per unit *ma*ss):

$$K = \frac{d\overline{E_{\mathrm{tr}}}}{dm}. \tag{15.65}$$

If we consider monoenergetic photons of energy $h\nu$ and consider only the interaction of the primary photon beam (not any secondary photons, such as Compton-scattered photons or annihilation radiation), then the kerma is

$$K = \frac{\mu_{\mathrm{tr}}}{\rho}\Psi, \tag{15.66}$$

where Ψ is the energy fluence. To see why this is true, note that if the N photons are spread over area S, then $NE = \Psi S$ and $dm = \rho S dx$. The kerma is

$$K = \frac{d\overline{E_{\mathrm{tr}}}}{dm} = \frac{\Psi S \mu_{\mathrm{tr}} dx}{\rho S dx} = \frac{\mu_{\mathrm{tr}}}{\rho}\Psi.$$

15.15.3 Energy Imparted and Absorbed Dose

The *energy imparted,* E, is the net energy into the volume from all sources: uncharged particles, charged particles, and changes of rest mass:

$$E = (R_{\mathrm{in}})_u - (R_{\mathrm{out}})_u + (R_{\mathrm{in}})_c - (R_{\mathrm{out}})_c + \sum Q. \tag{15.67}$$

The *absorbed dose* is the expectation value of the energy imparted per unit mass:

$$D = \frac{d\overline{E}}{dm}. \tag{15.68}$$

It is measured in joules per kilogram or *gray* (Gy).

15.15.4 Net Energy Transferred, Collision Kerma and Radiative Kerma

Another quantity used in the literature is the *net energy transferred*. It subtracts from the energy transferred the energy that is reradiated (bremsstrahlung and radiation from positron annihilation in flight), even if the reradiation takes place outside the volume of interest. It is

$$E_{\mathrm{tr}}^{\mathrm{net}} = (R_{\mathrm{in}})_u - (R_{\mathrm{out}})_u^{\mathrm{nonr}} - R_u^r + \sum Q. \tag{15.69}$$

The *collision kerma* and *radiative kerma* are defined as expectation values per unit mass:

$$\begin{aligned} K_C &= \frac{d\overline{E_{\mathrm{tr}}^{\mathrm{net}}}}{dm} = K - K_r, \\ K_r &= \frac{d\overline{R_u^r}}{dm}. \end{aligned} \tag{15.70}$$

Considering only a primary beam of monoenergetic photons,

$$K_C = \frac{\mu_{\mathrm{en}}}{\rho}\Psi. \tag{15.71}$$

15.16 Charged-Particle Equilibrium

There are three equilibrium conditions that sometimes exist or are assumed to exist, that make it possible to calculate the relationship between energy transferred and energy imparted.

15.16.1 Radiation Equilibrium

The first and most restrictive condition is *radiation equilibrium*. It is a useful model when considering an extended radioactive source that is distributed uniformly throughout some volume V (such as the body or a particular organ). The source is assumed to emit its radiation isotropically. The energy released to neutrinos is ignored. A point of interest within the large volume is surrounded by a smaller volume v. The volume v must be far enough from the edge of V so that any radiation emitted from v is absorbed before reaching the surface of V. The entire volume V is assumed to be of the same atomic composition and density. Because everything is isotropic, on average for every photon or neutron or charged particle entering volume v, another identical one leaves. This means that

$$\left(\overline{R}_{\mathrm{in}}\right)_c = \left(\overline{R}_{\mathrm{out}}\right)_c \tag{15.72a}$$

and

$$\left(\overline{R}_{\mathrm{in}}\right)_u = \left(\overline{R}_{\mathrm{out}}\right)_u. \tag{15.72b}$$

The average energy imparted is

$$\overline{E} = \sum \overline{Q}. \tag{15.73}$$

When the conditions for radiation equilibrium are satisfied, the absorbed dose is the expectation value of the energy released by the radioactive material per unit mass. If there is no radioactive source, there is no energy imparted in radiation equilibrium.

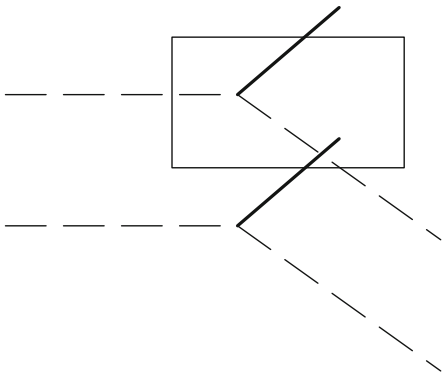

Fig. 15.33 One of the conditions for charged-particle equilibrium is that on average, for every charged particle of a certain energy leaving volume v traveling in a certain direction, a corresponding particle enters the volume

15.16.2 Charged-Particle Equilibrium

A less restrictive assumption is *charged-particle equilibrium*, in which only Eq. 15.72a is satisfied: the average amount of charged-particle radiant energy entering the region is the same as the average amount leaving. The assumption of charged particle equilibrium is a useful model in several cases, but we will consider only the case of an external beam of photons striking volume V. Again we consider what happens in a smaller volume v, separated from the boundary of V by a distance larger than the maximum range of any secondary charged particles produced by the external radiation. We also assume that the medium is homogeneous and that only a small fraction of the primary radiation interacts within the volume so attenuation can be neglected. Then the average number of charged particles produced per unit volume and per unit solid angle in any given direction is the same everywhere in the volume. Though the charged particles need not be produced isotropically, on average for every particle that leaves volume v, a corresponding one will enter it, as shown in Fig. 15.33. For charged-particle equilibrium, the average energy imparted is

$$\overline{E} = \left(\overline{R}_{\text{in}}\right)_u - \left(\overline{R}_{\text{out}}\right)_u + \sum \overline{Q}.$$

Comparing this with the average of Eq. 15.69 shows that the average net energy transferred is

$$\overline{E_{\text{tr}}^{\text{net}}} = \overline{E} + \left(\overline{R}_{\text{out}}\right)_u - \left(\overline{R}_{\text{out}}\right)_u^{\text{nonr}} - \overline{R_u^r}.$$

Now recall that $\left(\overline{R}_{\text{out}}\right)_u$ is the average value of all the uncharged radiation leaving volume v, $\left(\overline{R}_{\text{out}}\right)_u^{\text{nonr}}$ is the average value of all uncharged radiation leaving excluding bremsstrahlung and photons from annihilation in flight that occur within the volume, and $\overline{R_u^r}$ is the bremsstrahlung and annihilation-in-flight radiation from charged particles originating in v regardless of where it occurs. If there is charged-particle equilibrium, any radiative interaction by a charged particle after it leaves the volume will on average be replaced by an identical interaction inside v. If the volume is small enough so that all radiative loss photons escape from the volume before undergoing any subsequent interactions, then

$$\left(\overline{R}_{\text{out}}\right)_u = \left(\overline{R}_{\text{out}}\right)_u^{\text{nonr}} + \overline{R_u^r}.$$

Therefore, *for charged-particle equilibrium*, $\overline{E} = \overline{E_{\text{tr}}^{\text{net}}}$, and the dose is equal to the collision kerma:

$$D = K_C. \tag{15.74}$$

One situation where charged-particle equilibrium applies is for the thin slices in Fig. 15.30a. The electron ranges are so short (10 μm for a 25-keV electron) that a slice can be thin compared to $1/\mu$ and yet all the electrons produced stay within the volume.

The conditions for charged-particle equilibrium fail if the source of photons is too close (Ψ is not uniform because of $1/r^2$), close to a boundary (as between air and tissue or muscle and bone), for high-energy radiation (as in Fig. 15.32), or if there is an applied electric or magnetic field that alters the paths of the charged particles (as in some radiation detectors).

In Fig. 15.32, if we look at the situation far enough to the right, the energy imparted is proportional to the energy transferred. This situation is called *transient charged-particle equilibrium.*

The dose for a monoenergetic parallel beam of charged particles with particle fluence Φ passing through a thin layer can be calculated by making three assumptions:

1. The volume of interest is thin enough so that S_e remains constant.
2. Scattering can be neglected, so every particle passes straight through the layer.
3. The net kinetic energy carried out of the layer by δ rays is negligible, either because the layer is thick compared to the range of the δ rays or because the layer is immersed in a material of the same atomic number so that charged-particle equilibrium exists.

Then the energy lost in collisions in a layer of thickness dz is $E = \Phi(\text{area})(S_e/\rho)\rho dz$ and the mass is $\rho(\text{area})dz$, so the dose is

$$D = \frac{S_e}{\rho}\Phi. \tag{15.75}$$

Attix (1986, pp. 188–195) discusses corrections for situations where these assumptions are not valid.

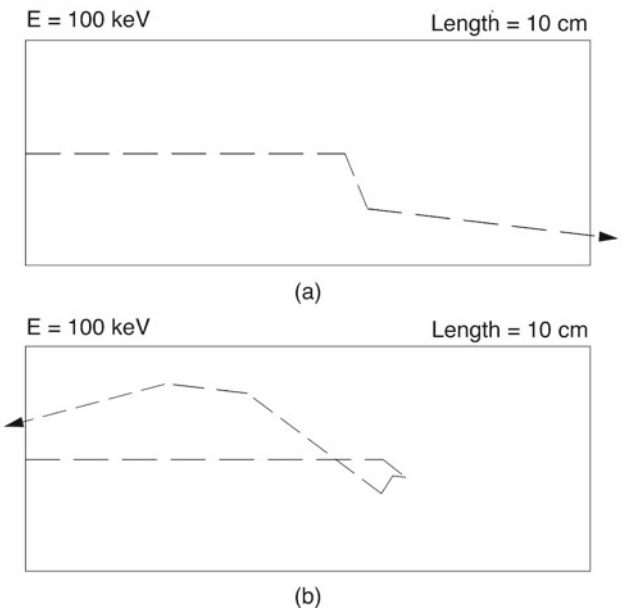

Fig. 15.34 Secondary photons also interact in this simulation. One 100-keV photon enters from the left in each panel. **a** The primary photon undergoes a Compton scattering. The Compton-scattered photon also undergoes a Compton scattering. The third photon escapes from the water. **b** The primary photon is Compton scattered. Each Compton-scattered photon undergoes another Compton scattering, until the sixth scattered photon leaves through the upstream surface of the water, traveling nearly in the direction from which the incident photon came

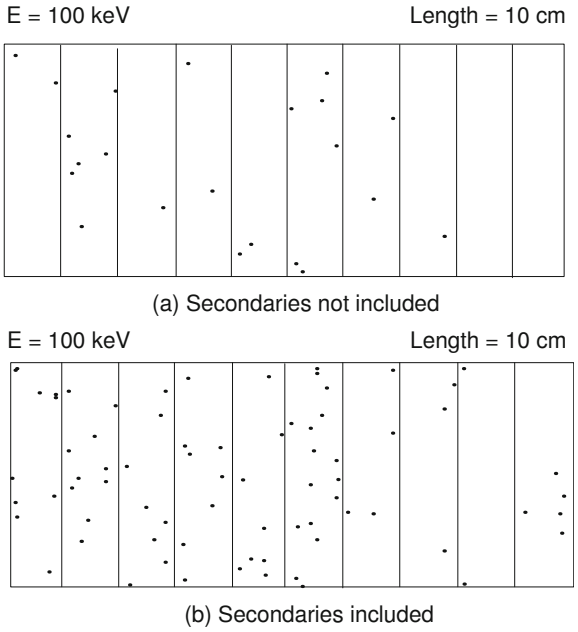

Fig. 15.35 Twenty-five 100-keV photons entered the water from the left. The dots represent recoil electrons from Compton scattering or photoelectrons. **a** Only the first interaction of the primary photon is considered. **b** Subsequent interactions are also considered

15.17 Buildup

We have been ignoring the interactions of secondary photons, primarily Compton-scattered photons and annihilation radiation. They can be quite significant. In fact, there can be a cascade of several generations of photons, though we will call them all *secondary photons*. Figure 15.34 compares two simulations in which the secondary photons are allowed to interact. In Fig. 15.34a there is one secondary interaction before the scattered photon escapes from the water. In Fig. 15.34b there are a total of six Compton scatterings before the secondary photon escapes.

All of these secondary photons produce electrons that contribute to the energy transferred and energy imparted. Figure 15.35 compares two cases where 25 photons of energy 100 keV enter the water from the left. The primary interactions are the same in both cases. In Fig. 15.35a the small dots represent the electrons produced by the interaction of the primary photons. In Fig. 15.35b the electrons produced by secondary and subsequent interactions are also shown. The energy transferred and energy imparted are much greater.

The *buildup factor* for any quantity is defined as the ratio of the quantity including secondary and scattered radiation

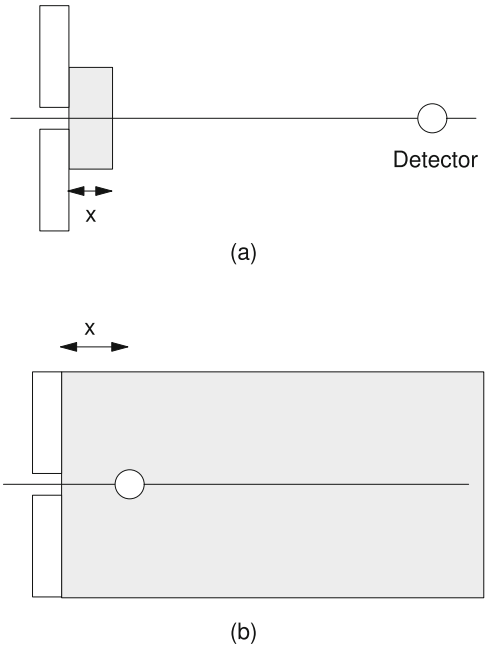

Fig. 15.36 Two different detector geometries. **a** The detector is at a fixed location and the absorber thickness is increased. **b** The detector is at a varying distance from the source in a water bath

to the quantity for primary radiation only. For example, if the primary beam has an energy fluence Ψ_0 at the surface, the energy fluence at depth x in the medium is

$$\Psi(x) = B(x)\Psi_0 e^{-\mu x}. \tag{15.76}$$

The buildup factor is quite sensitive to the geometry. Compare the two situations in Fig. 15.36. In Fig. 15.36a the detector is at a fixed location and the thickness of the absorber is increased. As the absorber thickness x approaches zero, the buildup factor approaches unity. In Fig. 15.36b the detector is at depth x in a water bath. Because of the backscattered radiation seen in Fig. 15.34b, $B(x) > 1$ as $x \to 0$. In this case, it is sometimes called the *backscatter factor*. For further discussion, see Attix (1986).

Symbols Used in Chap. 15

Symbol	Use	Units	First used page
a	Acceleration	m s^{-2}	440
a_i	Number of atoms of constituent i		434
b	Impact parameter	m	442
c	Velocity of light	m s^{-1}	428
d	Diameter	m	440
e	Charge on electron	C	425
f, f_C, f_i, f_κ, f_τ	Fraction of photon energy transferred to charged particles		431
g	Fraction of photon energy of secondary electrons converted back into photons by bremsstrahlung		437
h	Planck's constant	J s	427
j	Total angular momentum quantum number		425
k	Spring constant	N m^{-1}	440
l	Orbital angular momentum quantum number		425
m	Mass	kg	430
m_e	Electron rest mass	kg	428
m_j	Quantum number for the component of the total angular momentum along the z axis		425
m_0	Rest mass	kg	429
n	Principal quantum number		425
n	Number		434
p	Momentum	kg m s^{-1}	429
q	Charge	C	442
r	Position	m	444
r_e	"Classical" electron radius	m	430
s	Spin quantum number		425
t	Time	s	440
v	Velocity	m s^{-1}	439
w_i	Mass fraction of constituent i		434
x, y, z	Coordinate axes	m	433
x	Dimensionless energy ratio		430
z	Charge of projectile in multiples of e		439
A	Atomic mass number		433
A_i, A_{mol}	Atomic mass number of constituent i or molecule	(g mol)$^{-1}$ or (kg mol)$^{-1}$	434
A_K	Auger yield		435
B, B_K, etc.	Binding energy	eV or J	427
B	Buildup factor or backscatter factor		455
C	Shell correction coefficient		444
D	Absorbed dose	J kg^{-1} or Gy (gray)	452
E	Energy	J	426
E	Electric field	V m^{-1}	430
F	Force	N	440
F	Fraction of charged particles passing through an absorber		447
I	Average ionization energy	eV or J	444
I	Stopping interaction strength	J m^2	444
K, K_C	Kerma, collision kerma	J kg^{-1} or Gy (gray)	452
L	Stopping number per atomic electron		444
L_Δ	Restricted linear stopping power	J m^{-1}	447
M	Mass	kg	434
N	Number of particles		433
N_A	Avogadro's number	mol^{-1}	433
N_T	Number of target atoms per unit projected area	m^{-2}	434
N_{TV}	Number of target atoms per unit volume	m^{-3}	434
Q	Energy released from rest mass	J	451
R	Range	m	447
R_u, R_c	Radiant energy in the form of uncharged or charged particles	J	451
S	Area	m^2	452
S	Stopping power	J m^{-1}	439
S_e	Electron (collision) stopping power	J m^{-1}	440
S_n	Nuclear stopping power	J m^{-1}	440
S_r	Radiative stopping power	J m^{-1}	440
T	Kinetic energy	J	427
V	Volume	m^3	434
V	Velocity	m s^{-1}	443
$W_{K,L,M}$	Probability that a hole in the K, L, or M shell is filled by fluorescence		435
W	Energy lost in a single interaction	J	439
Y	Radiation yield		448
Z	Atomic number of target atom		425
β	v/c		439
δ	Average energy emitted as fluorescence radiation per photon absorbed	J	437
δ	Density-effect correction		444
ϵ	Stopping cross section	J m^2	439
ϵ_0	Electrical permittivity of free space	N^{-1} C^2 m^{-2}	430
θ, ϕ	Angles		429

κ	Pair production cross section	m^2	428
λ	Wavelength	m	429
μ, μ_{atten}	Attenuation coefficient	m^{-1}	433
μ_{en}	Energy absorption coefficient	m^{-1}	437
μ_{tr}	Energy transfer coefficient	m^{-1}	437
ν	Frequency	Hz	427
ξ	Position	m	443
ρ	Density	kg m^{-3}	433
σ_C	Total Compton cross section for one electron	m^2	427
σ_{coh}	Coherent Compton cross section for one atom	m^2	427
σ_{incoh}	Incoherent Compton cross section for one atom	m^2	427
σ_{tr}	Transfer cross section	m^2	431
σ_{tot}	Total cross section	m^2	433
τ	Photoelectric cross section	m^2	428
Δ	Energy transfer	J	447
Φ	Particle fluence	m^{-2}	436
Ψ	Energy fluence	J m^{-2}	436
Ω	Solid angle	sr	430

Problems

Section 15.1

Problem 1. The quantum numbers $m_s = \pm\frac{1}{2}$ and $m_l = l, l-1, l-2 \ldots, -l$ are sometimes used instead of j and m_j to describe an electron energy level. Show that the total number of states for given values of n and l is the same when either set is used.

Problem 2. Use Eq. 15.2 to estimate the K-shell energies for the following elements and compare them to the measured values of E_K.

Z	Element	Measured E_K (keV)
6	Carbon	0.284
20	Calcium	4.04
53	Iodine	33.2
82	Lead	88.0

Section 15.2

Problem 3. In the photoelectric effect, assume that the ejected electron has mass m and speed v and that the recoiling atom has mass M and speed V. Show that if the two particles have the same momentum, the kinetic energy of the atom is smaller than the kinetic energy of the electron by a factor (m/M). Calculate this factor for carbon and verify the claim in the text that the kinetic energy of the recoiling atom is small. Use non-relativistic expressions for the momentum and kinetic energy.

Section 15.3

Problem 4. The K-shell photoelectric cross section for 100-keV photons on lead ($Z = 82$) is $\tau = 1.76 \times 10^{-25}$ m^2 $atom^{-1}$. Estimate the photoelectric cross section for 60-keV photons on calcium ($Z = 20$).

Problem 5. Write Eq. 15.8 as $\tau = CZ^4E^{-3}$, where C is a proportionality constant. Estimate C from Fig. 15.3 (use $E = 100$ keV). Be sure to determine both the value of C and its units.

Problem 6. Describe how you could use different materials to determine the energy of monoenergetic x rays of energy about 50 keV by using changes in the attenuation coefficient. What materials would you use?

Section 15.4

Problem 7. Derive Eq. 15.11 from the preceding four equations.

Problem 8. Derive an equation for the direction of the recoil electron, ϕ, in terms of θ and λ_0.

Problem 9. A 1-MeV photon undergoes Compton scattering from a carbon target. The scattered photon emerges at an angle of 30°.

(a) What is the energy of the scattered photon? What is the energy of the recoil electron?

(b) What is the differential scattering cross section for scattering at an angle of 30° from one electron? From the entire carbon atom ($Z = 6$, $A = 12$)?

Problem 10. When $h\nu 0 >> mec^2$, what is the energy of a Compton-scattered photon at 180°? at 90°?

Problem 11. Integrate Eq. 15.16 over all possible scattering angles to obtain Eq. 15.18. Use the solid angle in spherical coordinates (Appendix L) and the substitution $u = 1 + x(1 - \cos\theta)$.

Problem 12. Integrate Eq. 15.17 over all possible scattering angles to obtain Eq. 15.19. Use the solid angle in spherical coordinates (Appendix L).

Problem 13. Find the limit of Eq. 15.16 as $x \to \infty$.

Problem 14. Write Eq. 15.16 in the form

$$\frac{d\sigma_C}{d\Omega} = \frac{r_e^2}{2}\left(1 + \cos^2\theta\right) F_{KN},$$

where F_{KN} is the *Klein–Nishina factor*. Find an expression for F_{KN} in terms of θ and x. Show that as $x \to 0$, $F_{KN} \to 1$. Show that when $\theta = 0$, $F_{KN} = 1$.

Problem 15. Use the expansion $\ln(1+x) = x - x^2/2 + x^3/3$ to show that Eq. 15.18 approaches Eq. 15.19 as $x \to 0$.

Problem 16. Eq. 15.11 shows that the wavelength shift is independent of the wavelength of the incident photon. Calculate the fractional wavelength shift $(\lambda - \lambda_0)/\lambda_0$ for an infrared photon ($\lambda_0 = 10$ μm), an ultraviolet photon ($\lambda_0 = 100$ nm), a low-energy ("soft") x ray ($\lambda_0 = 1$ nm), and a high-energy x ray ($\lambda_0 = 0.01$ nm).

Problem 17. Suppose that attenuation is measured for 60-keV photons passing through water in such a way that photons scattered less than 5° still enter the detector. Estimate the incoherent Compton scattering cross section per electron for photons scattered through more than 5°.

Section 15.5

Problem 18. A beam of 59.5-keV photons from ^{241}Am scatters at 90° from some calcium atoms ($A = 40$).

(a) What is the energy of a Compton-scattered photon?
(b) What is the energy of a coherently scattered photon?
(c) What is the recoil energy of the atom in coherent scattering?

Section 15.6

Problem 19. Show that a single photon cannot produce an electron–positron pair in free space because energy and momentum cannot be simultaneously conserved.

Section 15.7

Problem 20. Most diagnostic x rays use photon energies in the range 20–100 keV. For carbon (Fig. 15.2), which mechanism is most important in this range: photoelectric effect, Compton scattering, coherent scattering, or pair production?

Problem 21. Use Fig. 15.7 to make the following estimates for 1-MeV photons. What is the mass attenuation coefficient for water? For aluminum? For lead? What is the linear attenuation coefficient in each case?

Problem 22. Use Fig. 15.7 to estimate the attenuation coefficient for 0.1-MeV photons on carbon and lead. Compare your results to values you obtain from the internet or the literature. Repeat for 1-MeV photons.

Problem 23. Consider photons of three energies: 0.01, 0.02, and 0.03 MeV. What fraction of the photons at each energy will be unattenuated after they pass through 0.1 mm of lead ($\rho = 11.35$ g cm^{-3})? Comment on the differences in your results.

Section 15.8

Problem 24. Use Fig. 15.7 to find the mass attenuation coefficient for 0.2-MeV photons in a polyethylene absorber. The Compton effect predominates. Polyethylene has the formula $(CH_2)_n$.

Problem 25. What will be the attenuation of 40-keV photons in muscle 10 cm thick? Repeat for 200-keV photons.

Problem 26. Assume that a patient can be modeled by a slab of muscle 20 cm thick of density 1 g cm^{-3}. What fraction of an incident photon beam will emerge without any interaction if the photons have an energy of 10 keV? 100 keV? 1 MeV? 10 MeV?

Problem 27. Muscle and bone are arranged as shown. Assume the density of muscle is 1.0 g cm^{-3} and the density of bone is 1.8 g cm^{-3}. The attenuation coefficients are

E	$(\mu/\rho)_{\text{muscle}}$ (cm^2 g^{-1})	$(\mu/\rho)_{\text{bone}}$ (cm^2 g^{-1})
60 keV	0.200	0.274
1 MeV	0.070	0.068

Compare the intensity of the emerging beam that has passed through bone and muscle and just muscle at the two energies.

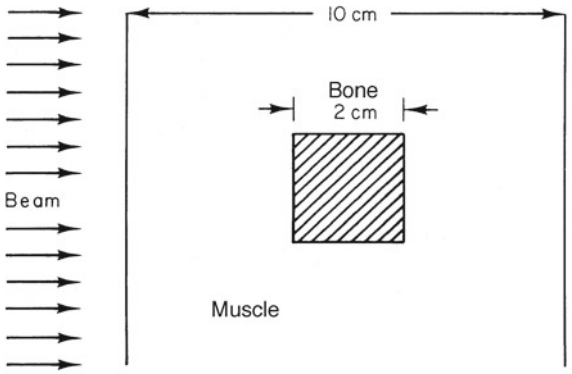

Problem 28. A beam of monoenergetic photons travels through a sample made up of two different materials of unknown thickness x_1 and x_2, as shown below. The attenuation coefficients at two different energies, E_a and E_b, are accurately known. They are $\mu_1(a)$, $\mu_2(a)$, $\mu_1(b)$, and $\mu_2(b)$. One measures accurately the log of the ratio of the number of photons emerging from the sample to the number entering, $R = \ln(N_0/N)$, at each energy so that R_a and R_b are known. Find an expression for x_2 in terms of R_a, R_b, and the attenuation coefficients.

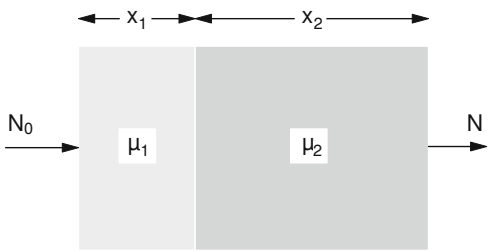

Section 15.9

Problem 29. The text showed that the mass atenuation coefficient for incoherent scattering is nearly independent of Z (assuming (Z/A) is constant). Show how the mass attenuation coefficient depends on Z for the photoelectric effect (use Eq. 15.8) and for pair production (assume $\kappa \propto Z^2$).

Problem 30. Use Table 15.1 to calculate the photon energies of the 13 spectral lines for tungsten that are shown in Fig. 15.13.

Problem 31. Use Table 15.1 and the selection rules in Eq. 15.32 to determine the allowed spectral lines for transitions in tungsten between M and N levels. Construct a drawing like that in Fig. 15.13 showing these transitions. Be sure to include the N_{VI} and N_{VII} levels in your drawing. Give these two levels slightly different energies so you can distinguish the transitions.

Problem 32. Use data from http://webelements.com/lead/orbital_properties.html to create a table like Table 15.1 and figures like Figs. 15.1 and 15.13, but for lead instead of tungsten.

Problem 33. You wish to use x-ray fluorescence to detect lead that has been deposited in a patient's bone. You shine 100-keV photons on the patient's bone and want to detect the 73-keV fluorescence photons that are produced. The incident photon fluence is $\Phi_0 = 10^{12}$ photons m^{-2}. There are 10^{14} lead atoms ($\approx$ 1 nmol) in the region illuminated by the incident beam. The photoelectric cross section is 1.76×10^{-25} m^2 atom^{-1}. The fluorescence yield is $W = 0.94$. Assume for simplicity that the fluorescence photons are emitted uniformly in all directions. The detector has a sensitive area 1×2 cm and is located 10 cm from the lead atoms. How many fluorescence photons are detected?

Section 15.10

Problem 34. A 5-keV photon strikes a calcium atom. The following events take place:

1. A K-shell photoelectron is ejected.
2. A K_α photon is emitted. This corresponds to the movement of a hole from the K shell to the L shell.
3. An electron in the M shell goes to the L shell and an M-shell electron is emitted.

Give the excitation energy of the atom, the total energy in the form of photons, and the total energy in the form of electron kinetic energy at each stage. Use the following data for calcium: $Z = 20$, $A = 40$, $B_K = 4000$ eV, $B_L = 300$ eV (ignore differences in subshells), $B_M = 40$ eV.

Problem 35. The following are the binding energies for hydrogen and oxygen.

	H	O
B_K	13.6 eV	532 eV
B_L		24 eV

(a) Determine f_τ for hydrogen from first principles.
(b) Use Eqs. 15.38 and 15.39 to estimate f_τ (K shell) for oxygen.

Problem 36. Use the Thomson scattering cross section, $d\sigma/d\Omega = (r_e^2/2)(1 + \cos^2\theta)$, the total cross section $\sigma_C = 8\pi r_e^2/3$, and the expression for the total energy of the recoil electron Eq. 15.15 to find an expression for f_C as $x \to 0$. Compare some values of $f_C \sigma_{C\,\text{incoh}}$ with the plot in Fig. 15.7.

Problem 37. (a) For 50-keV photons on calcium, estimate f_τ.
(b) For 100-keV photons on calcium, the photoelectric cross section is $\tau = 5.89 \times 10^{-28}$ m^2 atom^{-1}. Use $f_\tau = 1.0$. Estimate μ_{tr}/ρ. Use the following data for calcium if you need them: $Z = 20$, $A = 40$, $B_K = 4000$ eV, $B_L = 300$ eV, $B_M = 40$ eV.

Section 15.11

Problem 38. Prove that if a particle of mass M_1 and kinetic energy T collides head on with a particle of mass M_2 that is at rest, the energy transferred to the second particle is $4TM_2/M_1$ or $2M_2V^2$ in the limit $M_2 \ll M_1$. The maximum energy is transferred when the particles move apart along the line of motion of the incident particle.

Problem 39. The expression for $S_e = dT/dx$ has the SI units J m^{-1}. Therefore S_e/ρ in Eq. 15.56 has units J m^2 kg^{-1}.

(a) How must the coefficient in front of Eq. 15.56 be changed if T is in MeV? If x is in cm instead of m?
(b) What numerical factors must be introduced if N_A is in atoms per g mol and ρ is in g cm^{-3}?
(c) What is the average force on a 10-MeV proton in carbon? On a 100-keV proton? Use I=78 eV.
(d) What are the units of the stopping cross section (defined just below Eq. 15.46)?

Problem 40. The peak in the stopping power occurs roughly where the projectile velocity equals the velocity of the atomic electrons in the target. Find an expression for the velocity of an electron in the $n = 1$ Bohr orbit. Use Eq. 14.8, and the fact that the total energy is the sum of the kinetic and potential energies. Use the classical arguments and the fact that the electron is in a circular orbit to relate the kinetic and potential energies. The acceleration in a circular orbit is v^2/r.

Problem 41. A fishing lure is trolled behind a boat for a total distance D. Suppose that fish are distributed uniformly throughout the water at a concentration C fish m^{-3}, and that the probability of a fish striking the lure depends on b, the perpendicular distance from the path of the lure to the fish: $p = \exp(-b/b_0)$. Calculate the average number of fish caught.

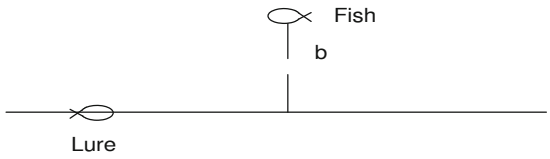

Section 15.13

Problem 42. What is the range energy relationship for high-speed non-relativistic particles if the variation of L with T is neglected and Eq. 15.56 is the dominant term?

Problem 43. Estimate the maximum electron range, and hence the radius of the δ-ray cloud surrounding the track of a 5-MeV α particle. (The rest energy Mc^2 of an α particle is about 4 times 938 MeV.) The range of a low energy electron in cm is about $10^{-2}\beta^2$.

Section 15.15

Problem 44. Suppose that a photon of energy $h\nu$ enters a volume of material and produces an electron–positron pair. Both particles come to rest in the volume, and the positron annihilates with an electron that was already in the volume. Both annihilation photons leave the volume. Show that the formal definition of energy transfer agrees with the common-sense answer that it is the kinetic energy of the electron and positron, which is $h\nu - 2m_e c^2$. What is the energy imparted?

Problem 45. What are the energy transferred, the net energy transferred, and the energy imparted in the volume shown?

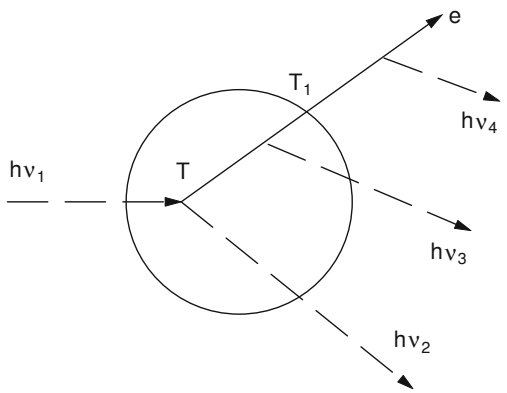

References

Ahlen SP (1980) Theoretical and experimental aspects of the energy loss of relativistic heavily ionizing particles. Rev Mod Phys 52:121–173

Arqueros F, Montesinos GD (2003) A simple algorithm for the transport of gamma rays in a medium. Am J Phys 71(1):38–45

Attix FH (1986) Introduction to radiological physics and radiation dosimetry. Wiley, New York

Bambynek W, Crasemann B, Fink RW, Freund HU, Mark H, Swift CD, Price RE, Rao PV (1972) X-ray fluorescence yields, Auger, and Coster–Kronig transition probabilities. Rev Mod Phys 44:716–813

Boone JM, Chavez AE (1996) Comparison of x-ray cross sections for diagnostic and therapeutic medical physics. Med Phys 23(12):1997–2005

Budd T, Marshall M (1983) Microdosimetric properties of electron tracks measured in a low-pressure chamber. Radiat Res 93:19–32

Carlsson GA, Carlsson CA, Berggren K-F, Ribberfors R (1982) Calculation of scattering cross sections for increased accuracy in diagnostic radiology. 1. Energy broadening of Compton-scattered photons. Med Phys 9(6):868–879

Hobbie RK (1992) MacDose: a simulation for understanding radiological physics. Comput Phys 6(4):355–359 (MacDose is available at the book web site https://files.oakland.edu/users/roth/web/hobbie.htm. It runs on a Macintosh computer using OS-9 or earlier)

Hobbie RK (2009) Photon interactions: a simulation study with MacDose. 26 minute video. https://itunes.apple.com/us/itunes-u/photon-interactions-simulation/id448438300?mt=10

Hubbell JH (1969) Photon cross sections, attenuation coefficients, and energy absorption coefficients from 10 keV to 100 GeV. NBS 29. US Govt. Printing Office, Washington DC

Hubbell JH (1982) Photon mass attenuation and energy absorption coefficients. Int J Appl Radiat Inst 33:1269–1290 http://dx.doi.org/10.1016/0020-708X(82)90248-4

Hubbell JH, Seltzer SM (1996) Tables of X-ray mass attenuation coefficients and mass energy-absorption coefficients 1 keV to 20 MeV for elements $Z = 1$ to 92 and 48 additional substances of dosimetric interest. National Institute of Standards and Technology. Report No. NISTIR 5632 Web Version. http://www.nist.gov/pml/data/xraycoef/index.cfm

Hubbell JH, Veigele WJ, Briggs EA, Brown RT, Cromer DT, Howerton RJ (1975) Atomic form factors, incoherent scattering functions and photon scattering cross sections. J Phys Chem Ref Data 4:471–538 (errata ibid. 6:615–616 (1977))

Hubbell JH, Gimm HA, Øverbø I (1980) Pair, triplet and total atomic cross sections (and mass attenuation coefficients) for 1 MeV–100 GeV photons in elements $Z = 1$ to 100. J Phys Chem Ref Data 9:1023–1147

Hubbell JH, Trehan PN, Singh N, Chand B, Mehta D, Garg ML, Garg RR, Singh S, Puri S (1994) A review, bibliography, and tabulation of K, L, and higher atomic shell x-ray fluorescence yields. J Phys Chem Ref Data 23(2):339–364

ICRU Report 16 (1970) Linear energy transfer. International Commission on Radiation Units and Measurements, Bethesda

ICRU Report 33 (1980) Radiation quantities and units. International Commission on Radiation Units and Measurements, Bethesda

ICRU Report 37 (1984) Stopping powers for electrons and positrons. International Commission on Radiation Units and Measurements, Bethesda. http://www.nist.gov/pml/data/radiation.cfm

ICRU Report 49 (1993) Stopping power and ranges for protons and alpha particles. International Commission on Radiation Units and Measurements, Bethesda. http://www.nist.gov/pml/data/star/index.cfm

Jackson JD (1999) Classical electrodynamics, 3rd edn. Wiley, New York

Jackson DF, Hawkes DJ (1981) X-ray attenuation coefficients of elements and mixtures. Phys Rep 70:169–233

Kissel LH, Pratt RH, Roy SC (1980) Rayleigh scattering by neutral atoms, 100 eV to 10 MeV. Phys Rev A 22:1970–2004

Powell CF, Fowler PH, Perkins DH (1959) The study of elementary particles by the photographic method. Pergamon, New York

Seltzer SM (1993) Calculation of photon mass energy-transfer and mass energy-absorption coefficients. Radiat Res 136:147–170

Tung CJ, Ashley JC, Ritchie RH (1979) Range of low-energy electrons in solids. IEEE Trans Nucl Sci NS-26:4874–4878

Ziegler JF, Manoyan JM (1988) The stopping of ions in compounds. Nucl Instrum Meth B B35:215–228

Ziegler JF, Biersack JP, Littmark U (1985) The stopping and range of ions in solids. Pergamon, New York